Frequency Offset Compensation in OFDM Transmission

Ruixuan He

A Thesis Presented to the Graduate Faculty

of the University of Virginia in Candidacy for the Degree of

Master of Science

Charles L. Brown Department of Electrical and Computer Engineering

University of Virginia

July, 2018

This thesis is dedicated to my parents,

Xieping and Yuwen.

Abstract

Orthogonal Frequency Division Multiplexing (OFDM) has been a signature technology in today's wireless communications such as Long Term Evolution (LTE) and Wireless Local Area Network (WLAN). With its high spectral efficiency, robustness in multipath environment, flexible allocation in subcarriers and other merits, OFDM provides higher transmission speed comparing to previous physical layer technologies. However, performance of the orthogonal and overlapping subcarriers in OFDM signal is highly vulnerable to poor frame synchronization that introduce Inter-Symbol Interference (ISI) and carrier frequency offset that results in Inter-Carrier Interference (ICI). In other words, without feasible algorithms for frame synchronization and frequency offset correction, OFDM may perform worse than previous technologies.

This research grows from an air-to-ground communications project in upper C band (between 5925-6700 MHz) with airborne test articles having a speed of up to Mach 2, or twice the speed of sound. This will introduce a large Doppler offset into the system and corrupt constellations if not well compensated. As a part of OFDM transmission study, the thesis will cover the background of OFDM systems, but mainly focus on frequency offset corrections for this type of implementations, analyzing how the frequency offset is introduced, how it would affect performance, comparing some frequency estimator performance, and the algorithms for compensation to get good constellations.

Acknowledgments

Foremost, I would like to express my sincere gratitude to my advisor Prof. Stephen G. Wilson, for his generous offer of this research opportunity, and his continuous support and guidance throughout my Master's study. I very much appreciate his patience and kindness during our discussions, and his motivation and dedication on my research.

Besides my advisor, I would like to thank the rest of my thesis committee: Prof. Maite Brandt-Pearce and Prof. Daniel S. Weller for devoting their time on my thesis committee

I feel grateful for the support of Laulima Systems, under contract to National Spectrum Consortium, for providing me with this chance of research.

I want to thank my groupmates and friends Rui Shang and Mrugen Deshmukh for their dedication, encouragement and companionship throughout my research.

I also would like to thank everyone at my Department and at University of Virginia, for their kindness and patience on helping me with my academic life throughout my Master's study.

Last but not least, I would like to thank to my parents, Xieping He and Yuwen Du, for their constant support and help on everything throughout my life.

Contents

List of Figures

List of Tables

Chapter 1

Introduction

As one of the signature technologies in Long-term Evolution (LTE), orthogonal frequency-division multiplexing (OFDM) has also been widely used as physical layer implementation for communications since 1990's in Digital Audio Broadcasting (DAB) and Asymmetric Digital Subscriber Line (ADSL) technologies. Yet evolution to OFDM began about 100 years earlier in the innovations during 1870s when Frequency-Division Multiplexing (FDM) was introduced for multiplying profits of telegraph companies [1]. It was not until late 1950's in North America that early development of OFDM appeared [2]. Then in 1970's, research indicated that, the Inverse Discrete Fourier Transform (IDFT) on data blocks produces a time domain signal to be a sum of modulated orthogonal subcarriers, which is OFDM modulation, and that a counterpart DFT serves as demodulation [3]. Thanks to practical implementations of Fast Fourier Transform (FFT) algorithm at same time, OFDM can be easily implemented in computer software for designing and simulating purposes and hardwares such as Digital Signal Processors (DSP), or field-programmable gate array (FPGA) chips for practical uses.

Comparing with its predecessor FDM with guard band between subchannels when doing parallel transmissions, OFDM employs overlapping but orthogonal frequency spectra, which boosts the spectral efficiency. Also, OFDM systems convert frequency-selective fading on a single carrier to flat-fadings on many subcarriers. This implies easier channel equalization. Besides, OFDM allows flexible designs according to mea-

sured channel conditions to fully make use of subchannels with high SNR i.e. one may use 2DPSK or 256QAM for different subchannels to allow for multiple data rates [4].

From above it is clear that OFDM's high performance mostly comes from its property of orthogonality between subcarriers. However, it is rather sensitive to distortions that occur in wireless channels because of large delay spread and carrier frequency offset. Large delay spread produces inter-symbol interference (ISI) which affects current symbol decisions and FFT orthogonality, so a cyclic prefix is introduced to combat it. Carrier frequency offset can be caused by oscillator drift at the transmitter or receiver, or Doppler shifts due to motion. Modern OFDM systems employs IDFT for modulation and DFT for demodulation, so it's vital to have reliable frame sync and Doppler offset compensations, otherwise, transmitted data can not be correctly recovered. **In this thesis, the main focus is on frequency offset estimation, compensation and performance analysis, for high-speed airborne-to-ground communications**.

1.1 Contribution

This research grew from a project for airborne-to-ground communication system that involves high-speed test articles with a velocity up to Mach 2. Hence, the main contribution of this thesis is studying, simulating and improving algorithms for Doppler frequency estimations and compensations in OFDM transmissions for the project. We implemented two previous algorithms that have different updating speed for both frame sync and frequency offset estimates and different detection ranges for Doppler offsets. Then we added some improvements for both in order to serve our project. For Sandell's algorithm [5], we simulated a method to expand the range for Doppler detection that has low complexity and good performance, making use of pilot subcarriers. For Schmidl's algorithm [6], we implemented a differential phase detector to refine frequency estimates. In addition, a general conclusion about unambiguous interval in OFDM Doppler estimation and its relations with frame sy-

chronizations will be discussed. Apart from those, a set of practical channel models including one or two-ray time-invariant, time-variant, and aircraft turning channels have been simulated for evaluating performance of algorithms in extreme cases with Doppler offsets.

1.2 Organization of the thesis

Chapter 1 gives a brief introduction of OFDM history, its pros and cons, and a brief overview of thesis structure. Chapter 2 deals with basic OFDM signal formation including cyclic prefix and subcarrier assignments, system diagrams and processing steps. Chapter 3 covers several types of distortions that a wireless channel will have on signal transmissions, with emphasis on the impact of frequency offset. In addition, two wireless channel models are introduced for practical simulations. Chapter 4 introduces two previous frequency offset estimation algorithms, and a method to expand unambiguous range for Sandell's estimator [5] with the aid of pilot subcarriers. Chapter 5 presents simulation results and shows performance of algorithms. Chapter 6 concludes the thesis and points out future works.

Chapter 2

OFDM Basics

This chapter covers some basic concepts and properties of OFDM communications, as a complement to the brief introductions in Chapter 1. As mentioned before, OFDM signal has a densely-packed overlapping spectrum with multiple subcarriers, which saves spectrum while perserving data, comparing to traditional FDM. Section 2.1 will formulate the OFDM signal. Section 2.2 deals with an important issue of OFDM symbols: prefixing sequence. In this section, two types of prefix: zero-padding and cyclic prefix, will be introduced and analysed. Section 2.3 presents a diagram of an OFDM system including transmitter, channel and receiver processing.

2.1 OFDM Signal

2.1.1 OFDM signal formation

Consider a QAM RF pulse being sent with a single carrier at frequency f_c:

$$s(t) = \Re\{\tilde{s}(t)e^{j2\pi f_c t}\}, \tag{2.1}$$

$\tilde{s}(t)$ is its complex envelope

$$\tilde{s}(t) = bp(t) \qquad 0 \leq t \leq T_d \tag{2.2}$$

where $p(t)$ is a rectangular pulse with an interval $T_d = 1/2$, and b is a complex QAM symbol. The RF spectrum of this pulse (Figure 2-1) has a width of $2/T_d = 4\ Hz$. if

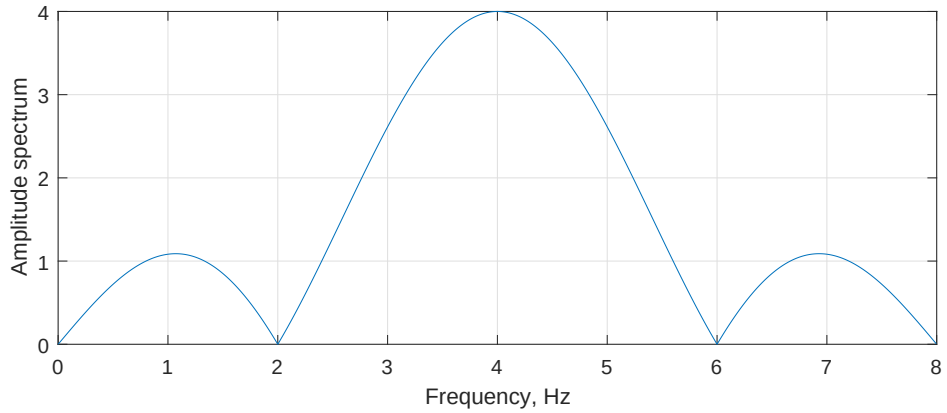

Figure 2-1: Amplitude spectrum of a rectangluar pulse

we divide this spectrum into four subcarriers, each subcarrier having bandwidth of $w = 2/4T_d = 1\ Hz$, and spacing $1/4T_d = 0.5\ Hz$, we get a spectrum of overlapping frequencies as described in Figure 2-2. At the same time, each subcarrier corresponds

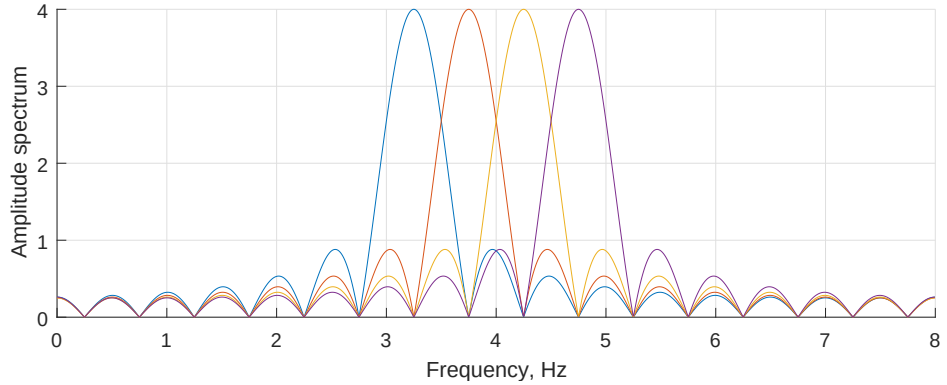

Figure 2-2: Four subcarrier spectrum obtained from the QAM pulse spectrum

with a time pulse of width $4T_d$, which means, the complex envelope of each pulse being:

$$\tilde{s}_i(t) = b_i g(t) e^{j2\pi\left[f_0' + \frac{i}{4T_d}\right]t} \qquad i = 0, 1, 2, 3;\ g(t) = p(t/4) \tag{2.3}$$

where f_0' is the frequency of the base subcarrier. Therefore, the complex envelope of OFDM signal is:

$$\tilde{s}_{ofdm}(t) = \sum_{i=0}^{3} b_i g_4(t) e^{j2\pi\left[f_0' + \frac{i}{4T_d}\right]t} \quad 0 \le t \le 4T_d;\ g_4(t) = p(t/4) \tag{2.4}$$

This can be extended to more subcarriers; if the spectrum of the QAM signal is divded into 8 overlapping and orthogonal subcarriers, the spectrum will look like

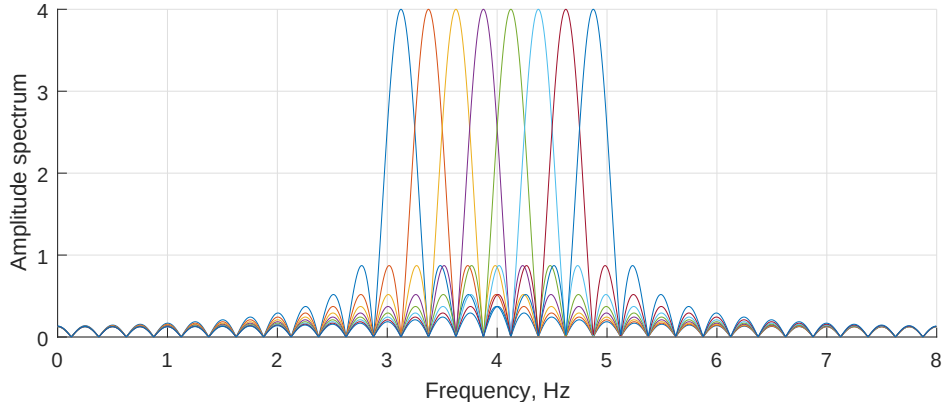

Figure 2-3: Eight subcarrier spectrum derived from the original pulse spectrum

This OFDM signal has 8 tones, or subcarriers, spaced by $1/8T_d = 0.25\ Hz$, each having a bandwidth of $2/8T_d = 0.5\ Hz$, And the time domain pulse will be 8 times longer at each subcarrier frequency. The corresponding complex envelope is

$$\tilde{s}_{ofdm}(t) = \sum_{i=0}^{7} b_i g_8(t) e^{j2\pi\left[f_0' + \frac{i}{8T_d}\right]t} \quad 0 \le t \le 8T_d;\ g_8(t) = p(t/8) \tag{2.5}$$

Figure 2-1 to Figure 2-3 show that within a same range of bandwidth, OFDM systems have multiple subcarriers, each employing a portion of the total bandwidth, where as single carrier systems assign the whole bandwidth to only one carrier. In the presence of multipath propagation (which will be introduced more in Chapter 3), the channel frequency response will vary with frequency. Figure 2-4 and 2-5 shows the frequency response of a two-ray multipath channel (red curves) with coherence bandwidth (a statistical measurement of the range of frequencies over which the channel can be considered "flat") of about one half of the total bandwidth. It can be seen that within

the band, the single carrier spectrum suffers from frequency-selective fading during transmission. whereas the OFDM system will have flat fading on each subcarrier.

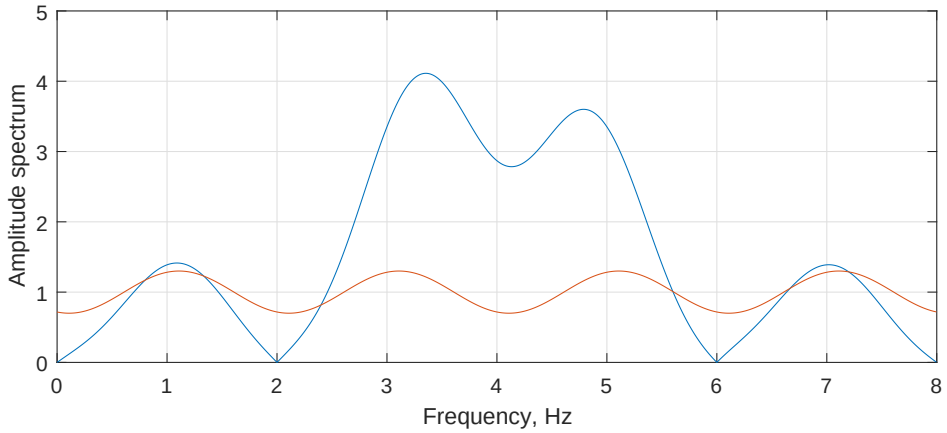

Figure 2-4: Single carrier signal spectrum with frequency selective fading

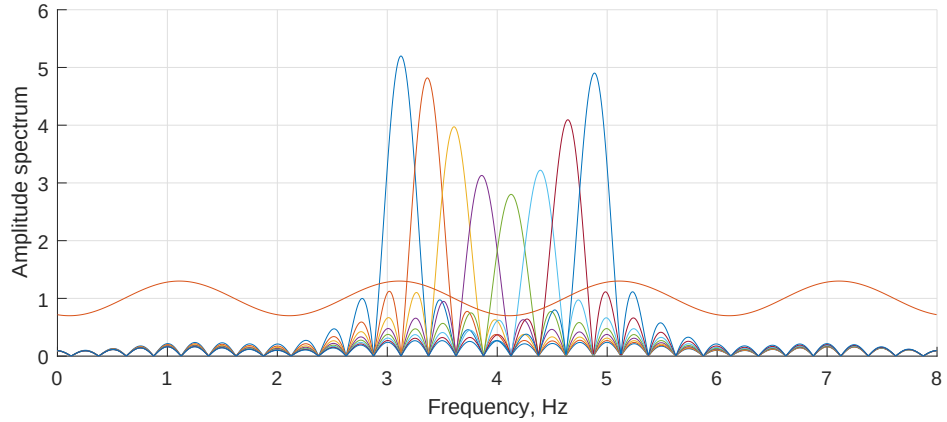

Figure 2-5: OFDM spectrum converts single carrier frequency-selective fading into subcarrier flat-fadings

In general, we have a complex envelope of an OFDM signal expressed as

$$\tilde{s}_{ofdm}(t) = \sum_{i=0}^{N-1} b_i e^{j2\pi \frac{i}{T} t}, \qquad 0 \leq t \leq T, \ i = 1, 2, ..., N \tag{2.6}$$

where i is the subcarrier index, N is number of subcarriers, and $1/T$ is the subcarrier

spacing. If sampled at $t = n\frac{T}{N}$, N times per symbol interval T, we have

$$\tilde{s}_{ofdm}(n\frac{T}{N}) = \sum_{i=0}^{N-1} b_i e^{j2\pi \frac{i}{T} n \frac{T}{N}} \tag{2.7}$$

which is

$$\tilde{s}_{ofdm}(n) = \sum_{i=0}^{N-1} b_i e^{j2\pi ni/N} \tag{2.8}$$

This indicates that the samples of the low-pass equivalent of the transmitted signal are given by IDFT of the subcarriers [8]. After the IDFT operation of each OFDM blocks, which is implemented as FFT in hardware, OFDM symbols in time domain are then serialized, with a guard time inserted between each symbol to prevent ISI from previous symbols due to multi-path dispersive channel. The length of guard time is chosen to be longer than the channel impulse response, so that tail of previous symbols won't show up in current FFT time. There are two types of guard interval:

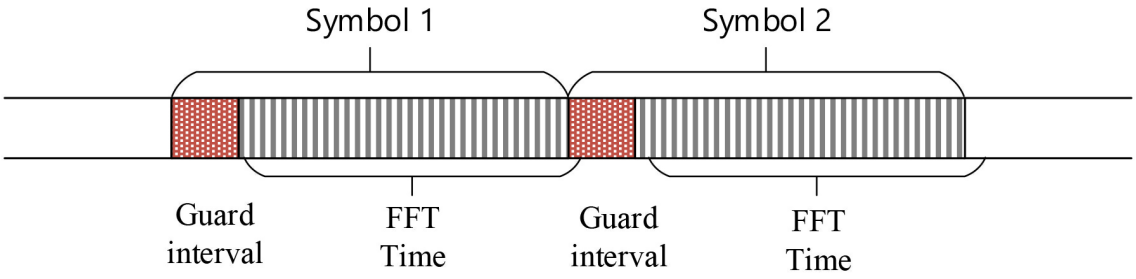

Figure 2-6: OFDM frame and guard time

zero-padding prefix and cyclic prefix. They will be introduced in the next section.

2.1.2 Cyclic prefix

To combat ISI from previous symbol in a dispersive channel, zero-padding is a method that is easier to implement, and can save more power when the guard interval needs to be very long, like in underwater OFDM communications, where it reduces the duty cycle for a practical transceiver [9]. However, more often the case is wireless communciation in the air, where complex gain of multipath can be significant relatively to the direct path. There a cyclic prefix is better in combatting

Inter Channel Interference (ICI). As is shown in Figure 2-8, signal with zero-padding guard interval will not suffer from ISI, but the multipath replica signal of the current OFDM symbol will introduce a zero amplitude period in the FFT time, which will result in ICI and distort the constellations. Figure 2-7 shows the formation of cyclic prefix, it is formed by copying the last L length samples to the front. The length L should be at least as long as channel impulse response.

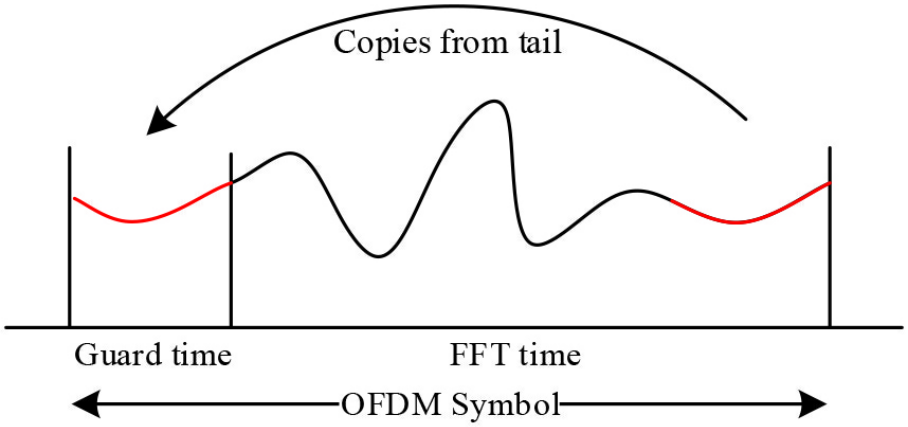

Figure 2-7: Cyclic prefix

Another function of cyclic prefix is that it preserves the multiplication of signal frequency spectrum and channel frequency response by property of cyclic convolution; i.e.

$$y(n) = x(n) \circledast h(n) + n(n) \tag{2.9}$$

$$Y(k) = X(k)H(k) + N(k) \tag{2.10}$$

where $y(n)$, $x(n)$, $h(n)$ and $n(n)$ are time domain received, transmitted, channel impulse response and noise signals, $Y(k)$, $X(k)$ $H(k)$, and $N(k)$ are their DFT's. The real channel is linearly convolving the transmitted signal with its impulse response. So cyclic prefix of the last samples of an OFDM frame serves as part of replica of the OFDM frame and make the channel's linear convolution appear as cyclic convolution. After dropping the cyclic prefix at the receiver, what's left is the sequence of cyclic convolution result $x(n) \circledast h(n)$, and hence in frequency domain, we have $Y(k) = X(k)H(k)$ as the received frequency spectrum. Channel equalization then calculates

$\hat{X}(k) = Y(k)/H(k)$ to recover the data. Apart from preserving data quality through

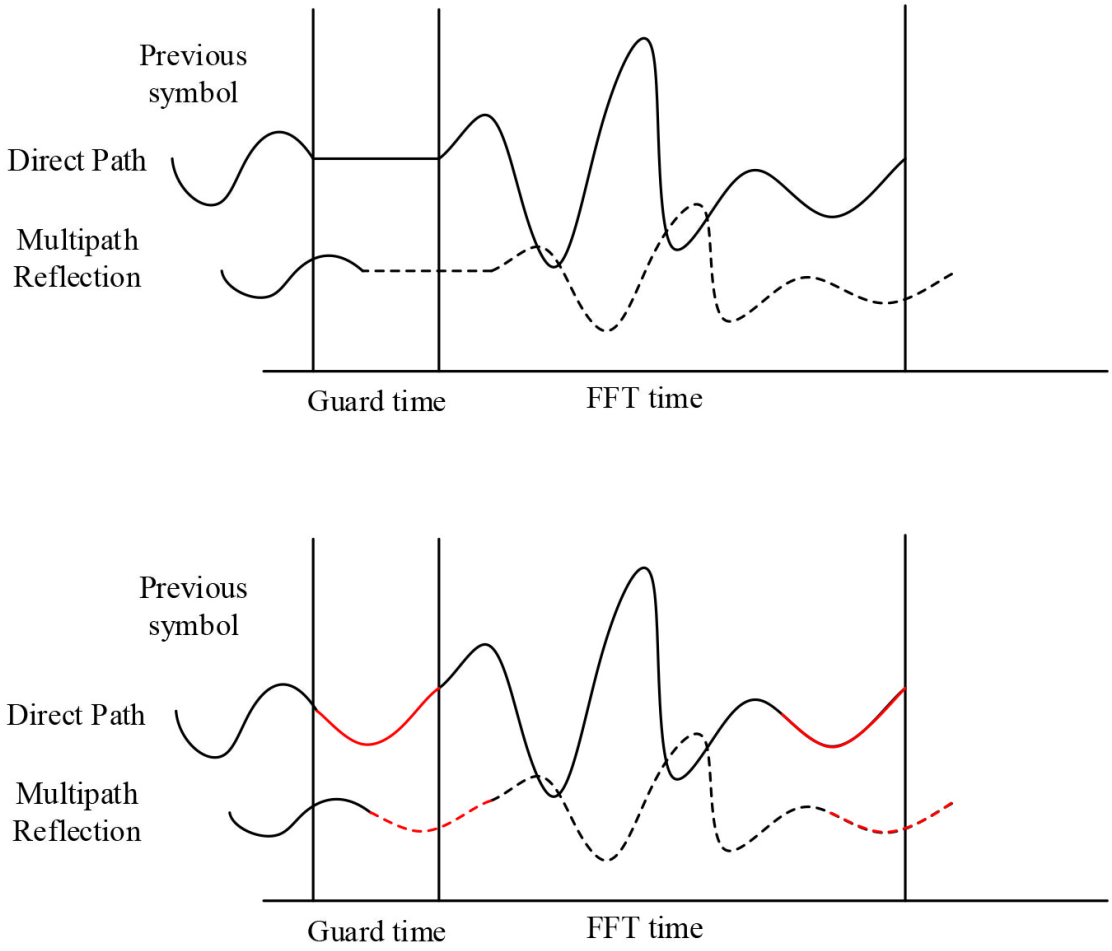

Figure 2-8: Comparison between zero-padded prefix and cyclic prefix

the channel, cyclic prefix provides the time domain signal with a repetition property that can be used for frame synchronization and frequency offset estimation [5], which will be covered in Chapter 4.

2.1.3 Subcarrier assignment

The cyclic prefix covered above is for preventing ISI and ICI and is an operation in time domain, after IFFT. Befor IFFT, in frequency domain, QAM symbols need to be assigned to subcarriers. An assignment example of subcarriers will be introduced in this subsection.

It is clear that OFDM system employs a set of subcarriers, with a total number

of N. One could assign these N subcarriers with data to be transmitted, but this way receiver will never know the distortions of the channel on signals. Certainly this is not feasible in practical cases. In today's OFDM systems, *pilot symbols*, known to the receiver, are assigned to subcarriers across the band, for measuring the channel frequency response by interpolating over all subcarriers, which provides channel estimation. Various channel estimation methods and their algorithm complexities are introduced in [10]. Also, pilot symbols can be used for estimating and compensating frequency offset, which will be covered in Chapter 4. Besides pilots, guard bands or "null subcarriers" are assigned at each edge of the band to protect the spectrum from spillage or spectrum spreading into adjacent systems. Assignment of OFDM subcarriers in our project is given in the Figure 2-9. There are in total $N = 128$ subcarriers, with 8 guard subcarriers on each side. A total number of 11 pilots are assigned uniformly across the band for better channel estimation results. 1 DC null subcarrier is assigned at the middle of the band.

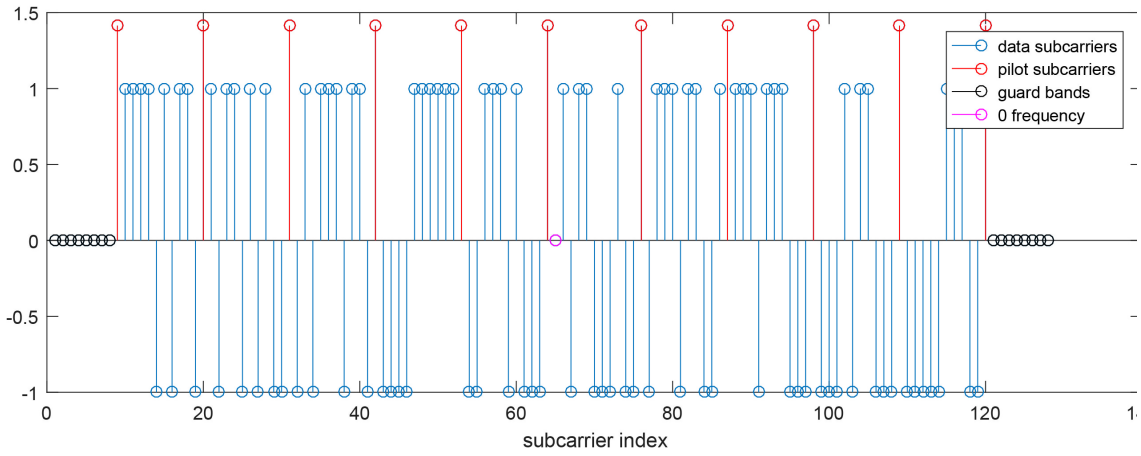

Figure 2-9: An assignment example of OFDM subcarriers, real part of X(k)

2.2 OFDM system diagram

OFDM transmitter and receiver diagrams are given in Figure 2-10, 2-11. At the transmitter, processing starts with generating QAM symbols from a serial data

stream. Then these symbols are inserted to data subcarriers, followed by pilot symbols and guard band insertions. After subcarrier assignments, this set of subcarriers are loaded into an N-point IFFT operation. The output of IFFT is the modulated time-domain OFDM signal with N subcarriers. Then, a cyclic prefix is inserted before each start of OFDM symbol. After that are upsampling and pulse shaping for transmission purposes. At the receiver, the received OFDM signal is first match filtered,

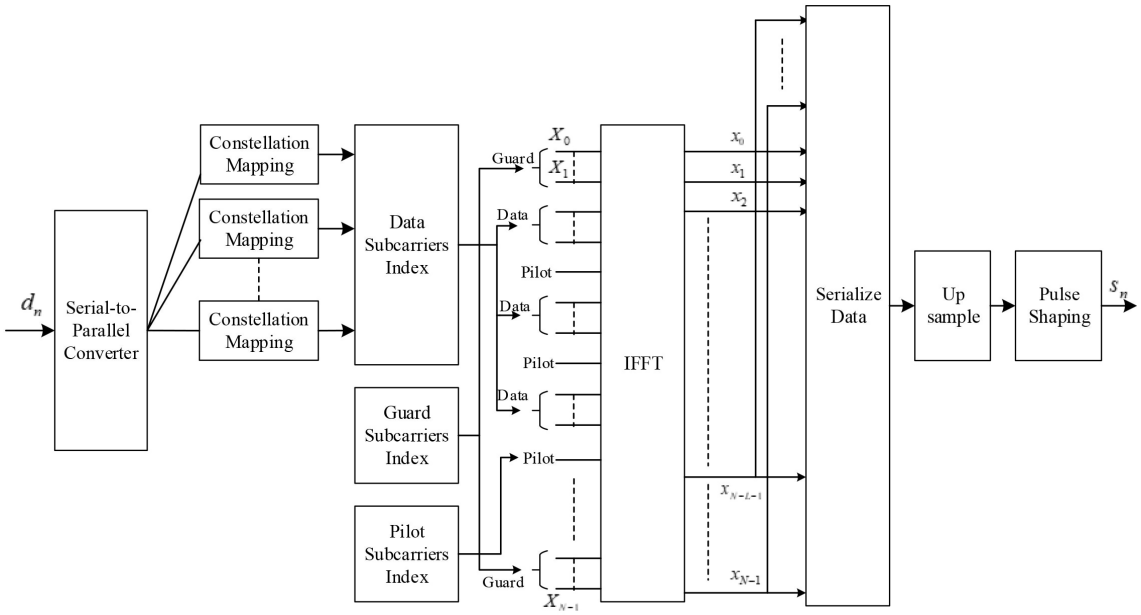

Figure 2-10: OFDM transmitter diagram

then gets downsampled. This down-converted sequence is then put into a symbol synchronizer, to find each OFDM symbol boundaries and frequency offsets which is the main focus of this thesis. After that, the down-sampled sequence is then parsed into OFDM symbols according to the time index produced by the symbol synchronization algorithm, with cyclic prefix dropped at the same time. Then each frame gets despinned, or frequency compensated, within each symbol. After that, each symbol then gets FFT demodulated, then with channel equalization, a constellation symbol is recovered. In our system for high-speed aircraft communications, there's a frequency ambiguity resolving process for handing large frequency offsets, see Figure 2-11.

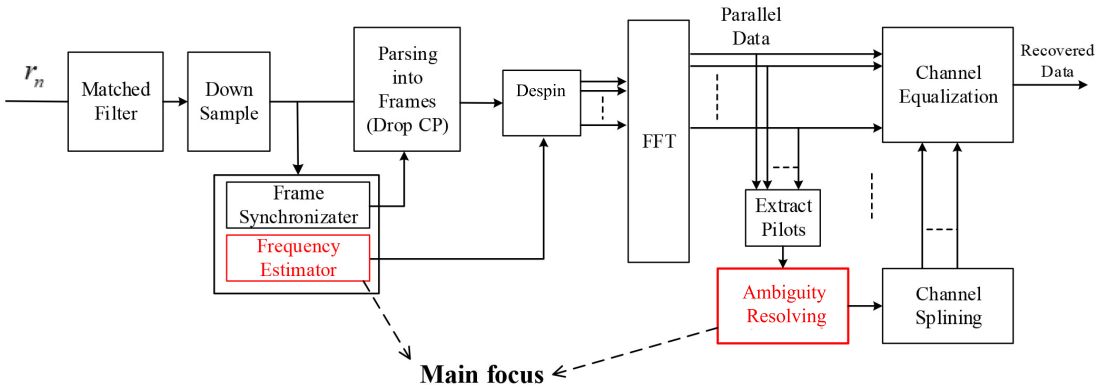

Figure 2-11: OFDM receiver diagram

Chapter 3

Wireless Channel

In any communication system, the transmission channel is a critical part because it is the pathway for information to pass through from transmitters to receivers. The RF signal will always be distorted when passing through a channel, and proper recovery at the receiver is needed. What's more, channels are different in various communication senarios, which affects signal and system designs.

In this chapter, propagation effects will be briefly introduced and analysed in section 3.1, including different types of signal power attenuations, their properties and mathematical models, with emphasis on multipath modeling and time-variant channel modeling. A time-variant channel is due to the motion of test articles, which introduces Doppler frequency offset. This, together with oscillator carrier frequency offset, lead to frequency offset in OFDM systems. In section 3.2, the effect of frequency offset in OFDM system is formulated and analysed, with constellation plots presented for illustration. Then in section 3.3, a two-path time-variant wireless model for communication between aircraft and a base station will be introduced and analysed, to practically simulate the channel. In section 3.4, a case study of aircraft turning is presented, for evaluating the time-variant property of the channel when an aircraft is making a turn from flying towards the base station to the opposite direction. Finally, section 3.5 briefly introduces channel noise modelling and scaling in our simulation.

3.1 Wireless channel attenuation

Based on the different mechanisms, wireless channel attenuations can be classified into four types: Path propagation loss, shadow effect loss, multipath fading, and time-variant fading. Path loss and shadowing effects attenuate the signal on a large scale of kilometers, whereas multipath and motion will result in fluctuations on signal strength in a small scale, in milliseconds. So we classify them into large and small scale fadings. Large scale fadings may be easier to mitigate by proper design of transmission power and better cellular coverage assignments. Small-scale fadings, happening on time intervals of the order of the symbol interval, or in frequency domain with order of signal bandwidth, are vital in receiver algorithm designs, in order to have smaller symbol error rates. Frequency estimation and compensation algorithms will be discussed in Chapter 4. In our air-to-ground communication project, shadowing is less important, and path propagation loss does not distort the signal in a fast manner, so these will be briefly introduced. Multipath effect and time-variant fading, however, are mostly involved for our applications and will be discussed more along with two typical channel models presented in section 3.3 and 3.4.

3.1.1 Path propagation loss

Path propagation loss is caused by free space signal propagation. One of the simplest mathematical model for this type of attenuation is the free space link equation, or Friis equation, that gives the received power P_r, with ideally matched antennas, as

$$P_r = \frac{P_t G_t G_r \lambda^2}{(4\pi d)^2} \tag{3.1}$$

where P_t is transmit power, G_t, G_r are gains at transmitter and receiver antennas, d is the distance, and λ the wavelength. However, statistical model for terrestrial wireless communications that takes terrain and shadowing into account gives a path loss model as [7]:

$$PL(dB) = PL(d_0) + 10n \log_{10}(\frac{d}{d_0}) \tag{3.2}$$

where n is the path loss exponent that depends on the environment, $PL(dB)$ is the path loss defined as:

$$PL(dB) = P_t(dB) - P_r(dB) \tag{3.3}$$

and $PL(d_0)$ is the path loss measure at a reference distance d_0. and is often taken to be the free space path loss at a distance of 10 meters [8].

3.1.2 Shadow fading

Shadow effect is illustrated by a mobile station moving on a circle with a radius of r, and experiencing variation in the blockage from trees, buildings and hills, etc. In this case, the received power can be expressed as [7]:

$$P_r(dB) = P_t(dB) + \sum_i \alpha_i(dB) \tag{3.4}$$

where α_i is the attenuation coefficient due to reflection and diffractions. Note each of α_i represents a a random and statistically independent attenuation, the summation approaches a Gaussian random variable, according to central limit theorem.

Now combining this with the path propagation loss model, the overall path loss is given by[7]:

$$PL(dB) = PL_{av}(dB) + X(dB) \tag{3.5}$$

where PL_{av} is obtained from the path loss model. Note shadow fading model is basing on a distance of a path propagation model, both of these two models accounts for large scale attenuations.

In addition to inevitable signal attenuation due to free-space loss, shadowing, diffractions, etc, an important wireless phenomenon is multipath propagation.

3.1.3 Multipath Modeling

Any wireless communication systems may suffer from multipath propagation effects, meaning apart from the direct path between transmitter and receiver, the signal will travel through many reflected paths and receiver will obtain replica signals

at different time based on the multipath distances, as is shown in the Figure 3-1. The combined signal including the direct path will appear to have Rayleigh fading envelope, which varys up to 30 dB over a very short time with order of millisecond [7]. In multipath propagation, the time duration between the direct path signal (or

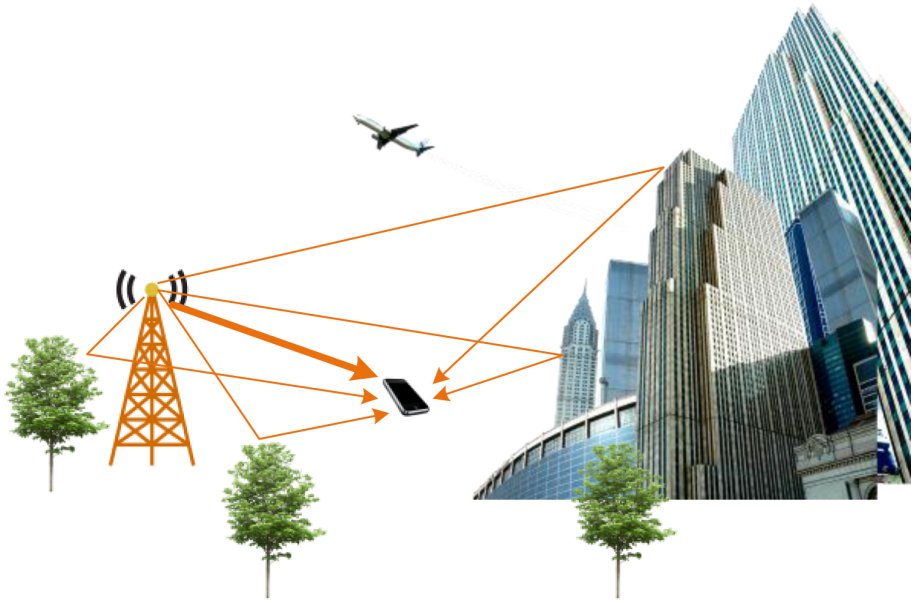

Figure 3-1: Multipath propagation

the first) and last significant replica of the signal arrives is called *delay spread*. An approximation of the reciprocal of delay spread is called coherence bandwidth, and is used to describe the interval of channel frequency response over which the response appears to be 'flat'.

Now for the simplicity, we illustrate a two-ray time-invariant multipath channel: with different delay of τ_1 and τ_2, and complex gain α_1, α_2. The channel impulse

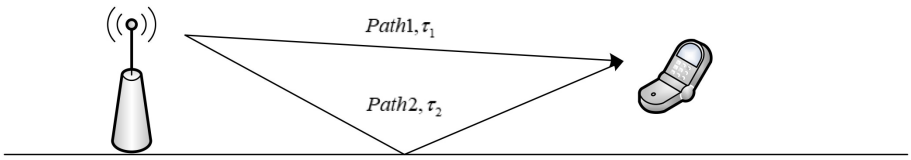

Figure 3-2: Multipath propagation

response is:

$$h(t) = \alpha_1 \delta(t - \tau_1) + \alpha_2 \delta(t - \tau_2) \tag{3.6}$$

Its frequency response is

$$H(f) = \alpha_1 e^{-j2\pi f\tau_1} + \alpha_2 e^{-j2\pi f\tau_2} \tag{3.7}$$

Let $H'(f) = H(f)e^{j2\pi f\tau_1}$, and $\tau = \tau_2 - \tau_1$, called delay spread, we have:

$$H'(f) = \alpha_1 + \alpha_2 e^{-j2\pi f\tau} \tag{3.8}$$

This two-ray $H'(f)$ is periodic in f with a period $1/\tau$. So in this case coherence bandwidth can be defined as approximatly $1/\tau$. If the signal bandwidth $W > 1/\tau$, then within the spectrum $H(f)$ has significant fluctuations, which is frequency-selective fading. If $W << 1/\tau$, then the channel gain will appear to be 'flat' across the band, and we say the signal experiences 'flat fading'.

To illustrate delay spread and coherence bandwidth, let's consider simulations with 0 Doppler offset, two and three paths. In the cases below, baseband sampling rate $f_s = 1\ MHz$, and the channel upsampling rate is $f_s' = 4\ MHz$

- Case 1 channel model: $h(t) = 0.9\delta(t) + 0.4\delta(t - \tau)$, delay spread: $\tau = 2\ \mu s$ (8 samples) $\Longrightarrow$ coherence bandwidth should be $1/\tau \approx 0.5$ MHz

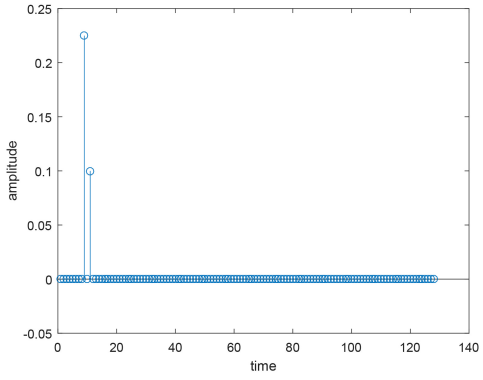

(a) Two path 2 μs delay impulse reponse (real part)

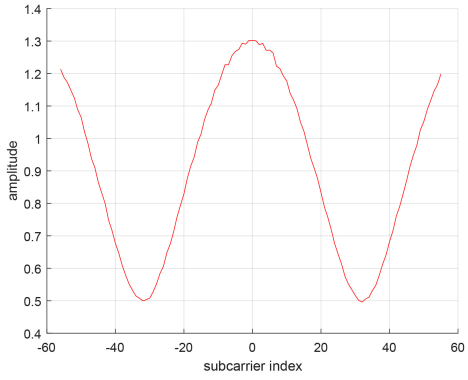

(b) Two path 2 μs delay frequency response (amplitude)

Figure 3-3: Two-path channel characteristic with 2 μs delay

Figure 3.3 (b) shows the channel frequency response after downsampling at $f_s = 1\ MHz$, with 128 subcarriers, and tone spacing is $F_{tone} = 1\ MHz/128 = 7812.5\ KHz$.

We can see at 2 μs delay, coherence bandwidth calculated from the channel frequency response is 64 tones, or $64 \times 7812.5\ KHz = 0.5\ MHz$, which checks the calculation above.

- Case 2 channel model: $h(t) = 0.9\delta(t) + 0.4\delta(t-\tau_1)e^{-j\pi/3} + 0.3\delta(t-\tau_2)e^{j\pi/4}$, delay spread: $\tau_1 = 2\mu s$ (8 samples) and $\tau_2 = 2\mu s$ (8 samples) $\Longrightarrow$ coherent bandwidth $B_c \approx 1/\tau = 0.25$ MHz

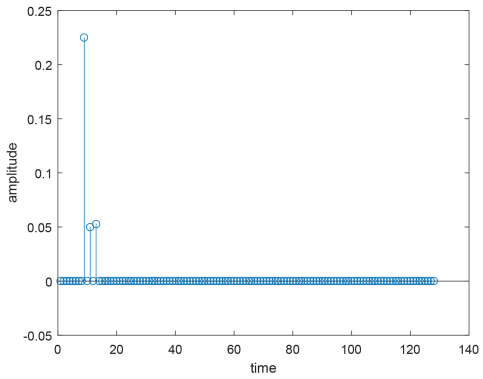

(a) Three path 4 μs delay impulse reponse (real part)

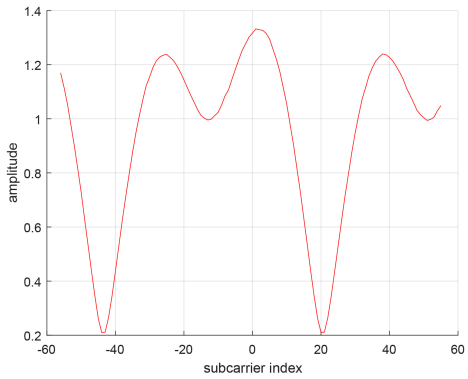

(b) Three path 4 μs delay frequency response (amplitude)

Figure 3-4: Three path channel characteristic with 4 μs delay

In Figure 3-4 (a), we can see the real part of impulse response of the second path is less than the third, this is due to the complex channel gain having a phase angle. And the right plot indicates a 'minicycle' of the channel frequency response to be 30 tone spacings, or coherent bandwidth $B_c = 30 \times 7812.5\ KHz \approx 0.234\ MHz \approx 1/\tau = 0.25\ MHz$.

3.1.4 Time-varying channel fading

Now consider a case when the transmitter and receiver have a relative speed towards each other, a typical example being communications between a moving mobile station and a static base station. Assuming a single carrier transmission with carrier frequency f_c, the transmitted signal $s(t) = Acos(2\pi f_c t)$, the received signal will have

a form

$$r(t) = Acos(2\pi(f_c + f_D)(t - t_D)) \tag{3.9}$$

where $f_D = \frac{\vec{\mathbf{v}} \cdot \vec{\mathbf{u}}}{c} f_c$, and where $\overrightarrow{\mathbf{u}}$ is the unit vector from mobile station to base station, $c = 3 \times 10^8\ m/s$ is the speed of light. So the signal spectrum will experience a shift, which is called Doppler shift. In air-to-ground communications, an aircraft will always have a large speed, comparing to ground transportations. This means a large Doppler shift is present and needs to be properly compensated. Otherwise, orthogonality of subcarriers can't be preserved. The effect of frequency offset will be formulated and analysed in section 3.2.

With multipath propagation, projections of speeds on different paths toward receiver can vary. This gives a combination of different speed and a spread on spectrum instead of a shift. Calculated from the relative speed from transmitter to receiver of each path, the difference between the maximum and the minimum Doppler frequency offset $B_D = f_{D_{max}} - f_{D_{min}}$ is called Doppler bandwidth, or Doppler spread. If the signal bandwidth is wide comparing to Doppler bandwidth, the signal spectrum suffers only slightly from the modulation from channel due to Doppler spread, and this kind of channel is called 'non-time-selective' channels, or 'slow fading' channel. Or if signal bandwidth is narrow comparing to Doppler bandwidth, the channel is 'time-selective' and signal will suffer from fast fading (this is atypical in modern wireless systems).

Significant Doppler spread is a tough case to handle, because it distorts the signal spectrum. In a two-path model, Doppler spread is due to two Doppler shifts, and the frequency synchronizer may synchronize at one of the path with larger channel gain. This gives frequency error and distorts the constellations. In the following section, frequency offset, its effect on constellations will be analysed and discussed.

3.2 Frequency offset effect in OFDM systems

Consider a complex envelope of an OFDM symbol produced by IDFT at transmitter, which is (2.8)

$$\tilde{s}(n) = \frac{1}{N}\sum_{i=0}^{N-1} b_i e^{j2\pi ni/N}, \quad n = 0, 1, ..., N-1 \tag{3.10}$$

where n is the sample index of the time-domain signal, and i is the subcarrier index. Let $\tilde{s}(t)$ be the complex envelope of continuous time signal. Assuming the signal experiences a frequency offset Δf during transmission, At the receiver, we have the complex envelope of the received signal as

$$\tilde{r}(t) = \tilde{s}(t)e^{j2\pi\Delta ft} \tag{3.11}$$

Sampling at $t = kT/N$, we have the received signal with Doppler as

$$\tilde{r}(n) = \frac{1}{N}e^{j2\pi\Delta f\frac{kT}{N}}\sum_{i=0}^{N-1} b_i e^{-j\frac{2\pi ni}{N}} \quad n = 0, 1, ..., N-1 \tag{3.12}$$

Then at the receiver, DFT demodulation gives frequency domain data sequence $X(m)$ =DFT$\big[\tilde{r}(m)\big]$, m is the frequency domain index after DFT

$$\begin{aligned}\tilde{X}(m) &= \frac{1}{N}\sum_{k=0}^{N-1}\left[e^{j2\pi\Delta f\frac{kT}{N}}\sum_{i=0}^{N-1} b_i e^{-j\frac{2\pi mi}{N}}\right]e^{-j2\pi\frac{km}{N}}, \quad m = 0, 1, ..., N-1 \\ &= \frac{1}{N}\sum_{i=0}^{N-1} b_i\left[\sum_{k=0}^{N-1} e^{j\frac{2\pi k}{N}\left(\Delta fT+i-m\right)}\right]\end{aligned} \tag{3.13}$$

Note in (3.13), the frequency offset appears in the phase angles of the received signal. We first illustrate the orthononality between subcarriers in OFDM, if there's no offset, let $\Delta f = 0$, we have

$$\tilde{X}(m) = \frac{1}{N}\sum_{i=0}^{N-1} b_i\left[\sum_{k=0}^{N-1} e^{j\frac{2\pi k}{N}\left(i-m\right)}\right] \tag{3.14}$$

Note in (3.14), i is the subcarrier index of the transmitted signal, and m is the subcarrier index of the demodulated signal. So if $i = m$, we have

$$\tilde{X}(m) = \frac{1}{N}\sum_{i=0}^{N-1} \cdot b_m = b_m \tag{3.15}$$

When $i \neq m$, then assume $i - m = l$, where l is an integer number, then (4.5) becomes

$$\begin{aligned} \tilde{X}(m) &= \frac{1}{N}\sum_{i=0}^{N-1} b_i \Big[\sum_{k=0}^{N-1} e^{j\frac{2\pi kl}{N}} \Big] \\ &= \frac{1}{N}\sum_{i=0}^{N-1} b_i \cdot 0 \\ &= 0 \end{aligned} \tag{3.16}$$

So without frequency offset, the orthogonality of the signal is preserved. If there is frequency offset $\Delta f \neq 0$, from (3.13) we have:

$$\tilde{X}(m) = \frac{1}{N}\sum_{i=0}^{N-1} b_i \Big[\sum_{k=0}^{N-1} e^{j\frac{2\pi k}{N}(\Delta fT + i - m)} \Big] \tag{3.17}$$

According to $\sum_{k=0}^{N-1} u^k = \frac{1-u^N}{1-u}$, and $-2jsinx = e^{jx} - e^{-jx}$, (4.8) can be simplified as

$$\begin{aligned} \tilde{X}(m) &= \frac{1}{N}\sum_{i=0}^{N-1} b_i \frac{1 - e^{j2\pi(\Delta fT + i - m)}}{1 - e^{j2\pi(\Delta fT + i - m)/N}} \\ &= \frac{1}{N}\sum_{i=0}^{N-1} b_i \frac{e^{j\pi(\Delta fT + i - m)}\left(e^{-j\pi(\Delta fT + i - m)} - e^{j\pi(\Delta fT + i - m)}\right)}{e^{j\pi(\Delta fT + i - m)/N}\left(e^{-j\pi(\Delta fT + i - m)/N} - e^{j\pi(\Delta fT + i - m)/N}\right)} \\ &= \frac{1}{N}\sum_{i=0}^{N-1} b_i e^{j\pi(\Delta fT + i - m)\frac{N-1}{N}} \frac{sin(\pi(\Delta fT + i - m))}{sin(\pi(\Delta fT + i - m)/N)} \end{aligned} \tag{3.18}$$

So the mth demodulated data symbol will have a form

$$\tilde{X}(m) = c_m b_m + \sum_{i=0, i\neq m}^{N-1} c_i b_i \tag{3.19}$$

where c_i is the contribution of each data $b_i, i = 0, 1, ..., N-1$ to the demodulated data, c_m and $c_i, i \neq m$ become

$$c_m = \frac{1}{N} e^{j\pi\Delta fT\frac{N-1}{N}} \frac{\sin(\pi\Delta fT)}{\sin(\pi\Delta fT/N)} \tag{3.20}$$

$$c_{i\neq m} = \frac{1}{N} e^{j\pi(\Delta fT+i-m)\frac{N-1}{N}} \frac{sin(\pi(\Delta fT+i-m))}{sin(\pi(\Delta fT+i-m)/N)} \tag{3.21}$$

Therefore, the mth demodulated symbol involves a summation of subcarriers $i = 0, 1, ..., N-1$ at the transmitter. This indicates inter-channel interference (ICI) and loss of orthogonality between subcarriers. Specifically, one can see on the right there's a scale factor

$$\frac{sin(\pi(\Delta fT+i-m))}{sin(\pi(\Delta fT+i-m)/N)} \tag{3.22}$$

and a phase angle

$$e^{j\pi(\Delta fT+i-m)\frac{N-1}{N}} \tag{3.23}$$

So in terms of constellations, its making noise-like scatter and at the same time, applying a rotation to the whole constellations.

To simulate this effect, we let the frequency offset normalized to tone spacing to be $\epsilon = \Delta fT$, and adjacent channel index to be $l = i - m$. Then we have

$$c_l = \frac{1}{N} e^{j\pi(\epsilon+l)\frac{N-1}{N}} \frac{\sin(\pi(\epsilon+l))}{\sin(\pi(\epsilon+l)/N)}, \quad l = 0,\ 1, ...\ N-1 \tag{3.24}$$

To illustrate, consider $N = 64,\ \epsilon = 0.05$. We show the real and imaginary part of the coefficients below. From Figure 3-5 (a) we see that the coefficients of adjacent channels introduce crosstalk to the decision of any channel. Figure 3-5 (b) shows at the current decision channel, there is a phase shift applied to it. This indicates the whole rotation of the constellation, which is shown in Figure 3-6.

Figure 3-6 shows the both rotation and scattering effect due to the coefficients. Also in figure 3-5 (b), we have the mth coefficient times a phase shift of 0.15 radians. This is 8.8 degrees, and is the rotation angle in figure 3-6.

Cases with larger frequency offsets are shown next.

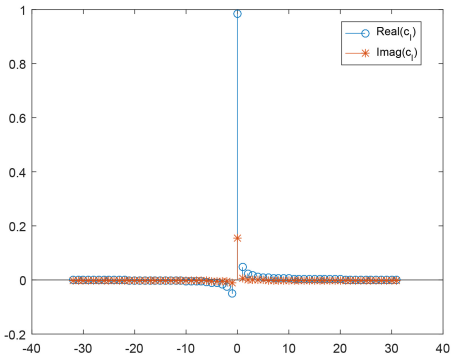

(a) Real and imaginary part of complex coefficients

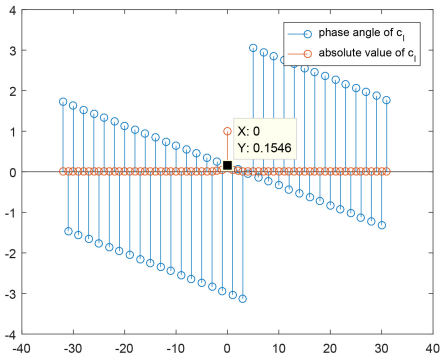

(b) Absolute value and angle of complex coefficients

Figure 3-5: Complex coefficients of l th adjacent subchannel

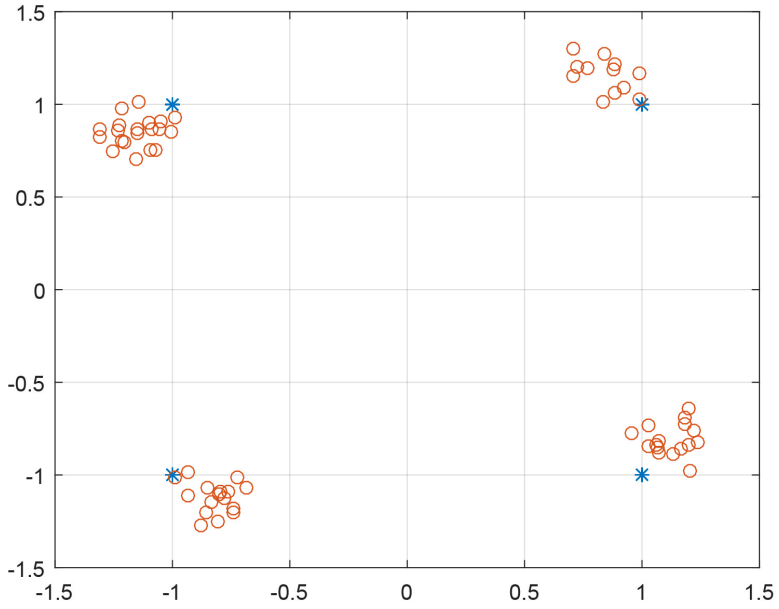

Figure 3-6: ICI and rotation in constellations due to frequency offset, $\epsilon = 0.05$

- $N = 64$, $\epsilon = 0.15$, (figure 3-7 (a))
- $N = 64$, $\epsilon = 0.20$, (figure 3-7 (b))

Note in real systems, pilots will also suffer from the rotation if frequency offset appears, which means channel equalization based on pilot interpolation is able to fix it. Yet the scattering due to ICI can not be taken care of. Imagine we rotate back the

constellations in above cases; the ICI scattering effect is still affecting decision. At $\epsilon = 0.2$ in figure 3-7 (b), we can see even if it is rotated back, the constellation is still bad for decision. So one may say $\epsilon = 0.2$ is a point that decision starts to degrade fast rapidly due to frequency offset. However, this is frequency offset only. In real channels, with presence of noise, we should aim to achieve frequency offset $\epsilon < 0.05$ to have proper constellations for decision.

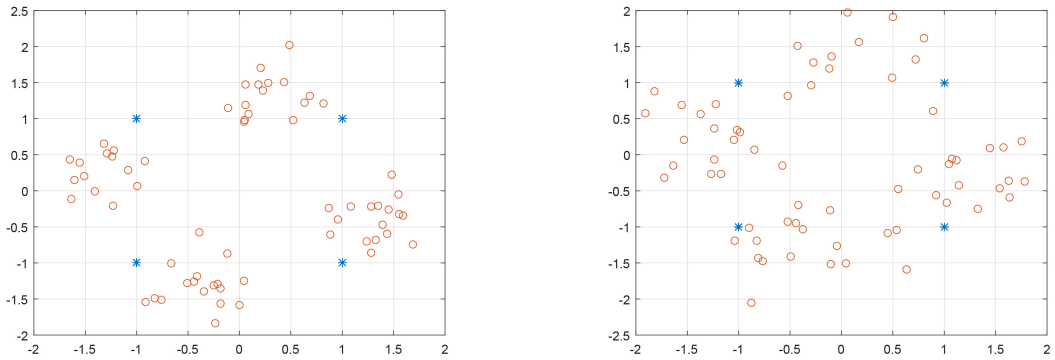

(a) Constellation with $\epsilon = 0.15$ (b) Constellation with $\epsilon = 0.20$

Figure 3-7: Frequency effect with different normalized offsets

In the above figures, constellations with frequency offset are plotted for one OFDM symbol. Next are the plots from several consecutive OFDM symbols. In Figure 3-8 and 3-9, each color denotes one OFDM symbol. We can see they experience rotations with different angles; this is due to the difference of propagation delay in time. Also, the scattering is because of ICI. Figure 3-9 shows a case with $\epsilon = 0.05$, we can see larger rotation and more scattering.

3.3 A channel model for aircraft communications

In this subsection, a two-ray multipath time-varing channel is introduced for simulation and testing purposes. Suppose we have two propagation paths from airborne terminal to the base station, with two distances being functions of time:

$$r_1(t) = r_0 + v_1 t \; meters \tag{3.25}$$

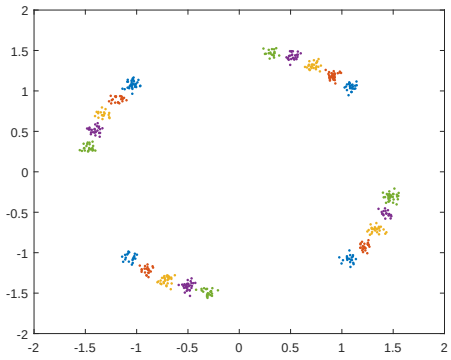

(a) Frequency offset effect across five consecutive OFDM symbols $\epsilon = 0.02$

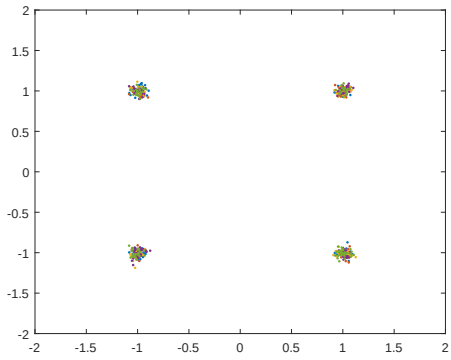

(b) Channel equalized five OFDM symbols with $\epsilon = 0.02$

Figure 3-8: Constellations of five consecutive OFDM symbols, with frequency offset $\epsilon = 0.02$

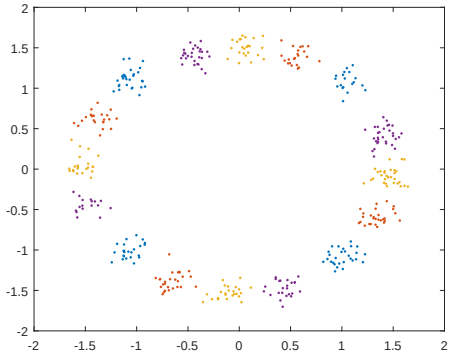

(a) Frequency offset effect across four consecutive OFDM symbols $\epsilon = 0.05$

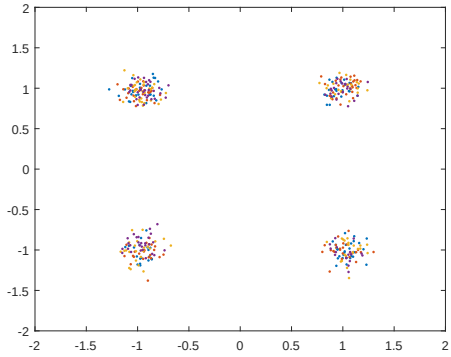

(b) Channel equalized four OFDM symbols with $\epsilon = 0.05$

Figure 3-9: Constellations of four consecutive OFDM symbols, with frequency offset $\epsilon = 0.05$

and

$$r_2(t) = r_0 + \Delta + v_2 t \ meters \tag{3.26}$$

where Δ is the initial differential range, and v_i are two velocities obtained from the assumed geometry. These can be generalized to allow a nonlinear change of range with time. To simulate this in discrete time at sampling rate f_s, we have

$$r_1[n] = r_0 + v_1 \frac{n}{f_s} \ meters \tag{3.27}$$

and

$$r_2[n] = r_0 + \Delta + v_2 \frac{n}{f_s} \; meters \tag{3.28}$$

Converting to time:

$$t_1[n] = \frac{r_0}{c} + v_1 \frac{n}{f_s c} \; seconds \tag{3.29}$$

$$t_2[n] = \frac{r_0 + \Delta}{c} + v_2 \frac{n}{f_s c} \; seconds \tag{3.30}$$

Now calculating the delay in samples:

$$D_1[n] = round\left[\frac{r_0 f_s + v_1 n}{c}\right]; \quad D_2[n] = round\left[\frac{(r_0 + \Delta) f_s + v_2 n}{c}\right] \tag{3.31}$$

Consider a generated transmitted signal $x(n)$, when passing through this channel, the received signal $r(n)$will be:

$$r[n] = a_1 e^{-j2\pi f_c t_1(n)} x(n - D_1(n)) + a_2 e^{-j2\pi f_c t_2(n)} x(n - D_2(n)) \tag{3.32}$$

This model involves motion of test articles and multipath propagation. So the delay spread is function of time. Also with a two-path time-variant channel, the Doppler frequency offset is not one but two. The difference between these two Doppler offsets is Doppler spread, which if a significant fraction of tone spacing, is hard for Doppler estimation algorithms to handle. In section 3.2 we saw a constellation with normalized frequency offset $\epsilon = 0.2$ gave poor constellations even after channel equalization. So if a case is the two propagation paths are introducing Doppler spread larger than $\epsilon = 0.2$, it is hard to compensate. This should be a research topic in the future. Luckily, in real world, multipath reflections with large gains are usually close to the direct path, thus the Doppler spread should be small. In our project, $\epsilon = 0.2$ corresponds to 1562 Hz. With such amount of Doppler, two paths will have a difference in speed of 78 m/s. Assuming a extreme case of Mach 2 for the test article, a difference of 78 m/s corresponds to an angle of a second path of $\arccos((680 - 78)/680) = 27.7$ degrees. This path should experience a large attenuation because of the range and angle, so the gain of this channel should be small, thus won't degrade constellation a lot.

3.4 Aircraft-turning model for studying Doppler rate

In section 2.1.3, the assignment of OFDM subcarriers are introduced, then in transmitter diagram in section 2.2, this one set of assignment will be IFFT modulated into a time-domain signal, then incerted with cyclic prefix. Recall in 2.1.2, cyclic prefix is mentioned to have a role in frame synchronization and frequency estimation, as is indicated in [5] and [11].

This indicates making use of cyclic prefix in each OFDM symbol, and updating estimates of frame sync and Doppler frequency offset symbol by symbol, which is employed in [5] and [11]. Note that [11] also made use of pilot subcarriers to achieve sharp peaks for OFDM symbol boundaries.

However, in many cases there is no need of updating the estimates symbol-by-symbol, because frequency is not changing that fast. For example, in the LTE standard [12], a typical frame length for an LTE frame is 10 ms. In our current project, the frame length is 30 ms. So it is unlikely that the frequency offset will change because the speed and direction of the aircraft will not change that fast. For example, let's use a typical acceleration of an aircraft catapult for calculation, that is 33 m/s^2, This gives a change in speed Δv of 0.33 m/s in 10 ms. At upper C band, pick a carrier frequency of $f_c = 8\ GHz$. So the Doppler change in this 10 $msec$ interval is:

$$\Delta f = \frac{\Delta v}{c} f_c = \frac{0.3364\ m/s}{3 \times 10^8\ m/s} \times 8 \times 10^9 Hz \approx 9Hz \tag{3.33}$$

Figure 3-10 illustrates the Doppler shift error across a frame duration of 10 ms, the estimate from the first symbol is introducing 9 Hz Doppler to the last symbol in the current frame, basing on the calculation above.

Note this 9 Hz offset to the constellation induces only a little bit ICI and will not affect decision making as is shown in Figure 3-11. Channel equalized constellation of 50 OFDM symbols with frequency error 500 Hz and 1000 Hz, single path, are given in Figure 3-12 for comparison. These two offsets are to 7812.5 kHz tone spacing $\epsilon_{500Hz} = 0.064$ and $\epsilon_{1000Hz} = 0.128$ when normalized. So it is feasible to estimate the start of frame and Doppler frequency offset once per frame rather than once per

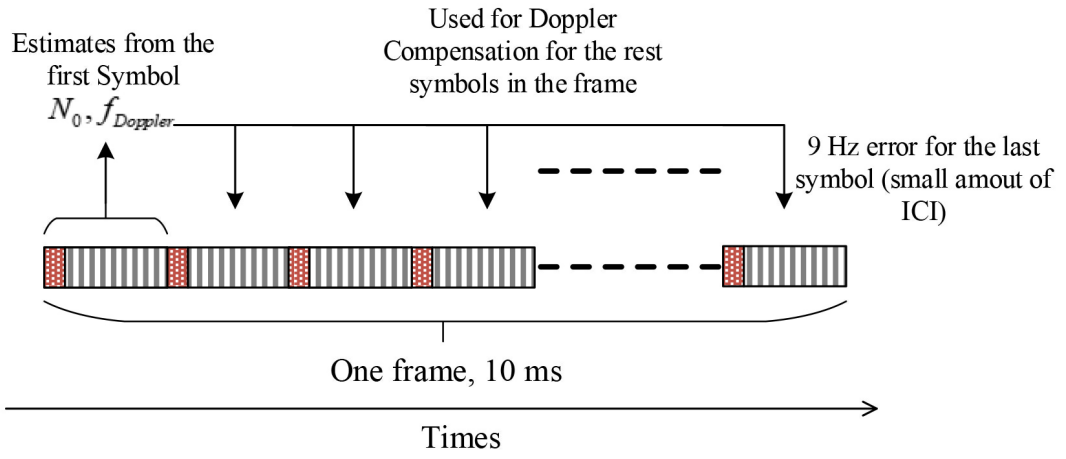

Figure 3-10: Using estimate from one symbol for compensating the rest of payload

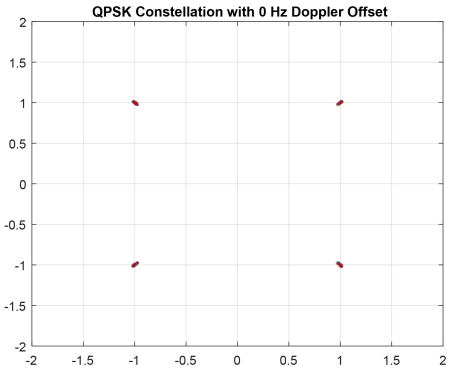

(a) 0 Hz Doppler Constellation

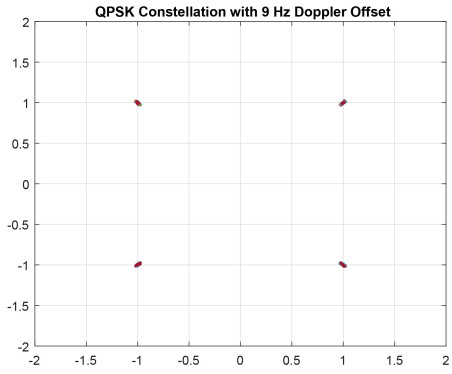

(b) 9 Hz Doppler Constellation for tone spacing 7.8125 kHz

Figure 3-11: Comparison between constellations with 0 Hz and 9 Hz Doppler offsets

OFDM symbol, which will save computation time.

However, whether this applies to a model of aircraft making turns needs to be verified. Note when an aircraft makes a turn from flying towards the base station to away, the Doppler frequency is changing from positive to negative, so how fast would this Doppler frequency offset change would be critical for adopting estimation once per frame or not, which is why the model in Figure 3-13 is being designed and analysed.

In this model, the aircraft is flying towards the base station at a constant speed v_0. Assume the turning radius is r, and the distance between the aircraft and the base

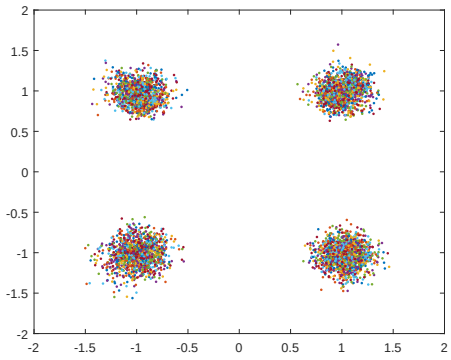

(a) Constellation of 500 Hz frequency error for tone spacing 7812.5 kHz ($\epsilon = 0.064$), single path

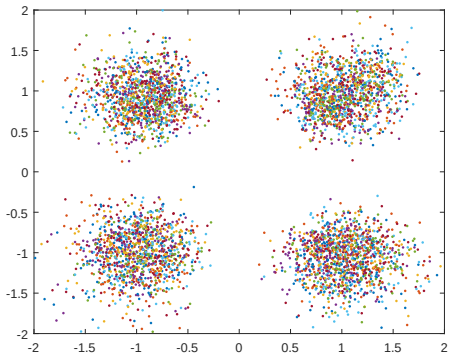

(b) Constellation of 1000 Hz frequency error for tone spacing 7812.5 kHz ($\epsilon = 0.128$), single path

Figure 3-12: Comparison between constellations with 500 Hz and 1000 Hz Doppler offsets

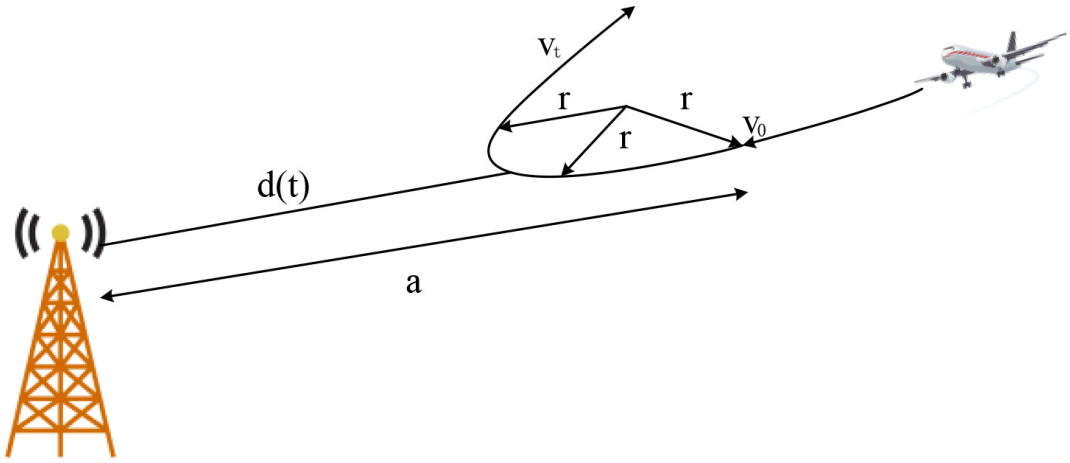

Figure 3-13: Aircraft turning model

station is $d(t)$. At time $t = 0$, the aircraft starts its turning process, and $d(0) = a$. At any time in the arc of turn, the distance between the center of the arc and base station is b, in simplified Figure 3-14, we have:

$$b = \sqrt{(a^2 + r^2)} \tag{3.34}$$

According to the law of cosines, the relationship between $d(t)$, r, and b, and the angle ϕ is:

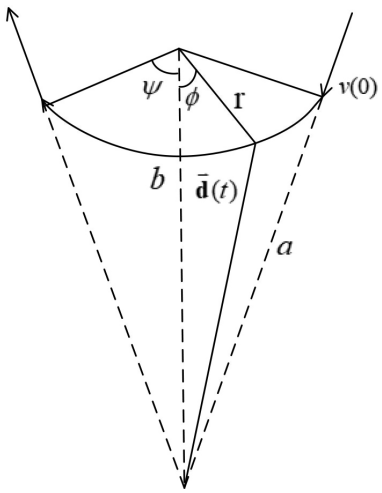

Figure 3-14: Aircraft turning physicalmodel

$$d^2(t) = b^2 + r^2 - 2br\cos\phi \tag{3.35}$$

Then to express the changing angle ϕ with a fixed angle ψ and the angular velocity ω :

$$\begin{cases} d^2(t) = \sqrt{b^2 + r^2 - 2br\cos\phi}, \\ \phi = \psi - \omega t \end{cases} \tag{3.36}$$

$$\Rightarrow d^2(t) = \sqrt{b^2 + r^2 - 2br\cos(\psi - \omega t)} \tag{3.37}$$

Then calculating the first and second derivative of $d(t)$, to obtain the vector of $v = d'(t)$, and $a = d''(t)$ where v and a both have a direction from the aifcraft towards the base station:

$$d'(t) = \frac{-\omega br\sin(\psi - \omega t)}{\sqrt{b^2 + r^2 - 2br\cos(\psi - \omega t)}} \tag{3.38}$$

$$d''(t) = \frac{\omega^2 br\cos(\psi - \omega t)}{\sqrt{b^2 + r^2 - 2br\cos(\psi - \omega t)}} - \frac{\omega^2 b^2 r^2 \sin^2(\psi - \omega t)}{\left[b^2 + r^2 - 2br\cos(\psi - \omega t)\right]^{\frac{3}{2}}} \tag{3.39}$$

Then the change of velocity with a direction towards base station is calculated over a frame time through:

$$\Delta v = d''(t) \cdot T_{frame} \tag{3.40}$$

The Doppler rate of change is

$$\frac{d(\Delta f)}{dt} = \frac{d''(t)}{c} \cdot f_c \tag{3.41}$$

Now we discuss a case of aircraft turning in terms of whether the maximum Doppler rate will produce untolerable Dopper estimation errors. Consider a case of aircraft having a speed of 900 m/s (slightly more than Mach 2). This is an extreme case since aircraft usually are slower when making turns. The turning path is a part of a circle, so we have a slow changing Doppler shift and Doppler rate, as is indicated in figure 3-15, as a function of the whole time of turning process, which is 80 *seconds*. We can see the Doppler shift is large at the begining of the turn, and is reduced when the aircraft is at the middle of making a turn, because the velocity is zero in the direction from test article to base station. The derivative of Doppler shift is Doppler rate.

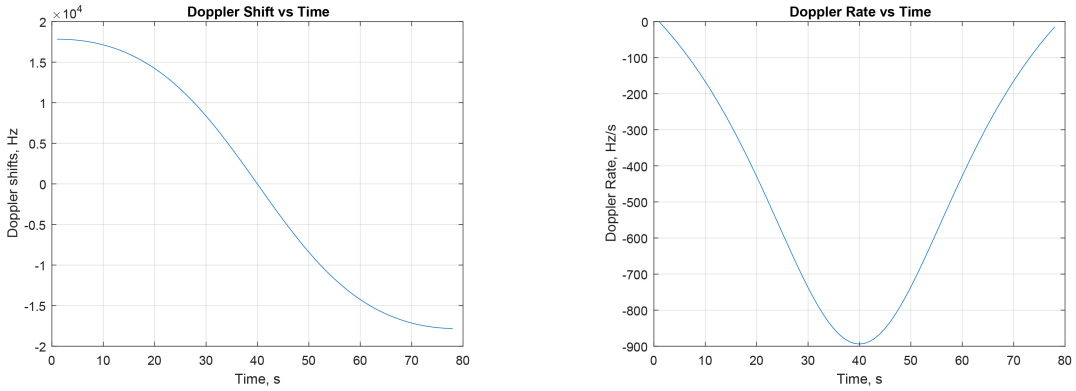

(a) Doppler shift vs time air-turning

(b) Doppler rate of change vs time

Figure 3-15: Doppler shift and rate change within turning process

Note that the frame time T_{frame} is small compared to turning time $T_{turning}$. We can pick an extreme value of Doppler rate during this turning process for calculation, which is -900 Hz, at the middle of the turning process. In our project, the frame length is 30 ms. So the Doppler change within this time interval is

$$\Delta f_{30ms} = -900Hz/s \times 30 \times 10^{-3}s = -27Hz \tag{3.42}$$

which according to previous analysis, is a very small amount of scattering for constellations. So we can say that we don't need to worry about Doppler variation across the frame.

3.5 Channel noise

Channel noise is another distortion that will degrade the system performance. It can be defined as unwanted (and usually uncontrollable) electrical signals interfering with the desired signal. [8] In the project, we model the channel with additive white Gaussian noise, and measure noise level by calculating E_b/N_0 in dB. The signal power at the receiver input is normalized to 1 with units joules/sample. To this signal we added complex Gaussian noise with variance each dimension σ_1 to be proper for our normalized signal power.

Chapter 4

Frequency Offset Estimation in OFDM

After reviewing OFDM basics and wireless channels, we now discuss algorithms for frequency offset estimation. In section 4.1, two previous frequency estimation algorithms [5] and [6] that we implemented are introduced and compared. These methods exploits correlation property of the received signal for frame timing and frequency offset estimation. Apart from these, [13] proposes a blind estimation technique using RBN with Probabilistic Neural Networks (PNN) for discriminating the frequencies of the carriers to compensate the effect of the frequency offset. [14] proposed a preamble structure whose energy serves as one of main criterions in frequency offset estimation. These points to different ideas on frequency offset estimation. In this thesis, we focus on algorithms introduced in section 4.1. Growing from those, section 4.2 introduces improvements for both algorithms for different purposes. For Sandell's algorithm, improvement is expanding the range of Doppler detection for high-speed airborne test article in our project, making use of pilot subcarriers. For Schmidl's algorithm, improvement involves a differential phase detector to refine the frequency estimates across frames. After that, section 4.3 discuss a general conclusion of frequency unambiguous interval that appears in estimating and compensating for large Doppler offset in OFDM systems.

4.1 Doppler estimation algorithms

In this section, two previous frame synchronization and Doppler estimation algorithms that we implemented and studied and defined are introduced and compared, Both algorithms have their pros and cons, and will be discussed in terms of two estimation schemes: symbol-by-symbol estimation and frame-by-frame estimation.

4.1.1 Symbol-by-symbol estimation

Recall in section 2.1.1 and 2.1.3, it is mentioned that after IDFT modulation, we obtain a time-domain OFDM sequence with length N, and then a cyclic prefix of length L is inserted for preventing ISI. This sequence including the cyclic prefix with length $N + L$ is called an OFDM symbol, and this subsection discuss methods for symbol-by-symbol estimation using cyclic prefix [5].

The principle of this timing and frequency synchronizer is to exploit the correlation property of the received signal $r(k) = (s(k-\theta) + n(k-\theta))e^{j2\pi\epsilon k/N}$ with cyclic prefix, where ϵ is normalized frequency offset relative to tone spacing which is $\epsilon = \Delta f T$. Note the cyclic prefix is a repetition of last few samples inserted into the begining of the OFDM symbol, and correlation of a shifted signal will produce correlation peak when the sample index is within the cyclic prefix.

$$E\{r(k)r^*(k+m)\} = \begin{cases} \sigma_s^2 + \sigma_n^2, & m = 0 \\ \sigma_s^2 e^{j2\pi\epsilon}, & m = N \\ 0, & \text{otherwise} \end{cases} \tag{4.1}$$

where $\sigma_s^2 \triangleq E\{|s(k)|^2\}$, and $\sigma_n^2 \triangleq E\{|n(k)|^2\}$ In [5], the log-likelihood function for timing estimate θ and frequency estimate ϵ is given as the logarithm of the conditional probability density function of observing the $2N + L$ samples in $\mathbf{r}$

$$\Lambda(\theta, \epsilon) = log\Big(\prod_{k \in CP} f\big(r(k), r(k+N)\big) \prod_{k \notin CP} f(r(k)) \Big) \tag{4.2}$$

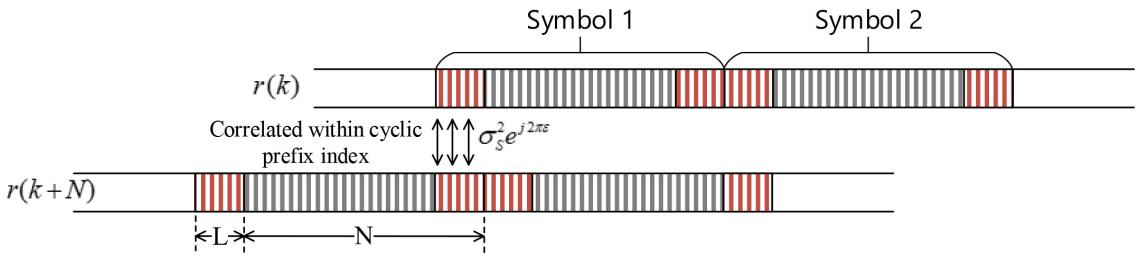

Figure 4-1: An illustration of correlation between $r(k)$ and $r(k+N)$

Simplifing the above gives the combined log likelihood as

$$\Lambda(\theta,\epsilon) = \sum_{k=\theta}^{\theta+L-1} \left(2Re\Big\{ e^{j2\pi\epsilon} r(k) r^*(k+N) \Big\} - \rho\Big(|r(k)|^2 + |r(k+N)|^2 \Big) \right) \tag{4.3}$$

where $\rho = \frac{\sigma_s^2}{\sigma_s^2+\sigma_n^2}$. Then, maximum likelihood estimates are computed from two steps: first compute the ML estimate of ϵ with respect to θ, then, compute the ML for θ

$$\max_{\theta,\epsilon} \Lambda(\theta,\epsilon) = \max_{\theta} \max_{\epsilon} \Lambda(\theta,\epsilon) = \max_{\theta} \Lambda(\theta, \hat{\epsilon}(\theta)) \tag{4.4}$$

Then two estimates are computed by

$$\hat{\theta} = arg\max_{\theta} \lambda(\theta), \quad \hat{\epsilon} = -\frac{1}{2\pi}\gamma(\theta)\Big|_{\theta=\hat{\theta}} \tag{4.5}$$

where

$$\lambda(\theta) = 2\left| \sum_{k=\theta}^{\theta+L-1} r(k) r^*(k+N) \right| - \rho \sum_{k=\theta}^{\theta+L-1} \left(\big|r(k)\big|^2 + \big|r(k+N)\big|^2 \right) \tag{4.6}$$

$$\gamma(\theta) = \angle\left(\sum_{k=\theta}^{\theta+L-1} r(k) r^*(k+N) \right) \tag{4.7}$$

In a simulated case with number of subcarriers $N = 128$, and length of cyclic prefix $L = 20$, sampling rate $f_s = 1\ MHz$, and input frequency offset to be 1000 Hz and no white Gaussian noise has been added, we get the estimator output in Figure 4-2. Looking at the upper subplot, one can tell the maximum value of timing estimator has an interval of approximately 148, which is equal to the OFDM symbol length,

and the peaks appears to be "noisy" due to random data. At timing index $\lambda = 41$, we have a frequency offset output $\epsilon = 0.128$. Recall that $\epsilon = \Delta f T$, and this T is the total time of signal duration before IDFT modulation and is sampled by N points in order to be modulated to N subcarriers, so $T = T_{ifft}$, and frequency offset can be computed by

$$\Delta f = \frac{\epsilon}{T_{ifft}} = \epsilon \cdot F_{tone} \tag{4.8}$$

where $T_{ifft} = N_{ifft} \cdot f_s = 128 \times 10^{-6}$ s is the IFFT time, and tone spacing is $F_{tone} = 1/T_{ifft} = 7812.5$ Hz. Therefore we have the estimated Doppler as $\Delta f = 0.128 \times 7812.5$ $kHz = 1000$ Hz as expected. It should be mentioned that peaks in

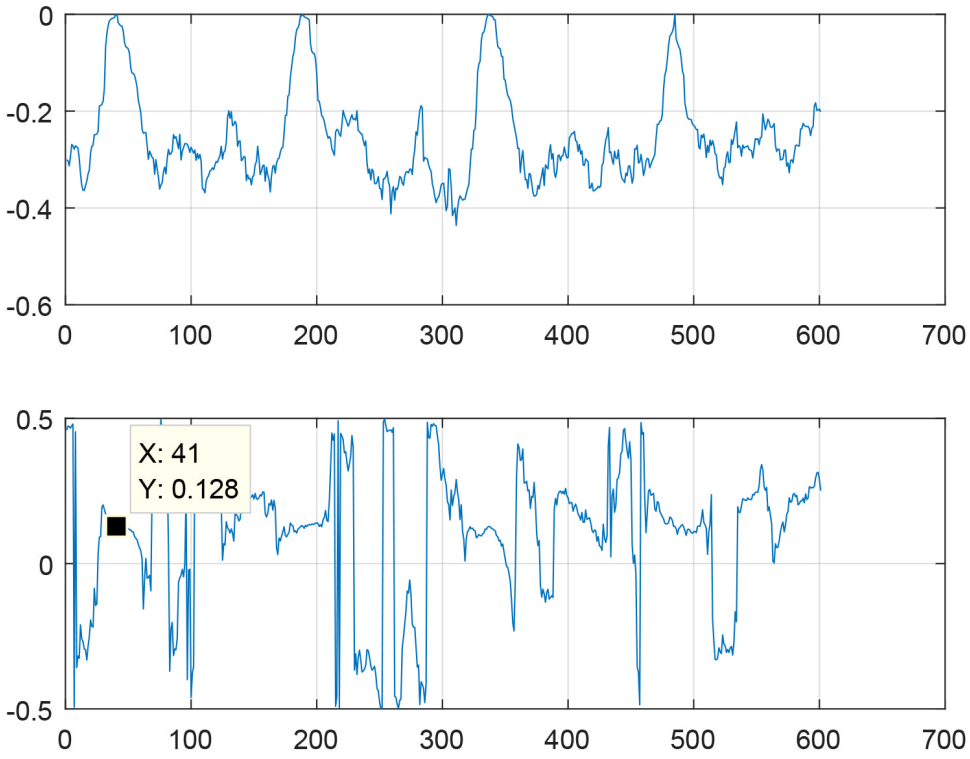

Figure 4-2: Sandell's estimator output with conditions $N = 128$, $L = 20$ Doppler offset=1000, $SNR = 80$ dB

Sandell's paper [5] the peaks are relatively sharper than what we have here because a longer OFDM symbol was implemented and more power is contributed to estimations. Performance on root-mean-square error of frequency estimates will be presented in

Chapter 5.

In low SNR cases, the peak of timing estimator sometimes is less accurate, especially in short OFDM symbol settings that is designed in our project. This means we need to extract more power from the signal for frame sync algorithm; in [11] we employed pilot signals buried in OFDM symbol, combined with cyclic prefix, to achieve a sharper peak [11] especially for low SNR case. This part of our research will be reported in my colleague Rui Shang's work.

Note in Sandell's algorithm, the estimated frequency can only be half of the tone spacing, i.e. $\Delta f < \pm(1/2)F_{tone}$, as one can see from the second subplot. This range of detection is suitable for most low-speed communication cases. System designers may change the symbol duration to achieve larger tone spacings. However, for high speed air-to-ground communications, we will encounter aircraft with a speed as high as Mach 2, or 680 m/s which converted into Doppler is

$$\Delta f_{v=mach\ 2} = \frac{680\ m/s}{3 \times 10^8\ m/s} \times 6 \times 10^9 = 13.6\ kHz \tag{4.9}$$

So we need to expand the range of this algorithm in terms of frequency estimator, which will be discussed in section 4.3.

4.1.2 Frame-by-frame estimation

In this subsection, we discuss another frame sync and frequency estimation algorithm from Schmidl and Cox [6]. The difference between this algorithm and the one in section 4.1.1 is that this one does not rely on a cyclic prefix. It introduces two OFDM symbols for frame sync and Doppler estimation that can be assigned before OFDM payload symbols and serves as the start of a long protocol frame. Therefore, it can be seen as a frame-by-frame estimation scheme.

The advantage of this is certainly less computation. For each OFDM protocol frame, it only computes one set of estimates, and uses them to compensate for the rest of the payload symbols. On the other hand, if the duration of a protocol frame is relatively long compared to channel coherence time (a time duration over which

the channel impulse response is considered to be not varying), the estimates at the beginning of protocol frame may not compensate for payload well. More importangly, making use of two specifically designed OFDM symbols, this metric can estimate frequency larger than one tone spacing, which is applicable to high-speed scenarios.

The rest of this subsection will briefly introduce this algorithm and generally compare this with Sandell's. Performance analysis will be presented in Chapter 5.

In Schmidl's algorithm, a time-domain training symbol designed with two identical halves is used to search for symbol timing. After transmission, these two identical parts should still have same amplitude, except for variations because white Gaussian noise. As for frequency, samples at the same location in the first and the second half should experience a phase shift of $\phi = \pi \Delta f T$, where $T = T_{ifft}/2$, as is indicated in Figure 4-3. Let N be number of samples for IFFT modulation, so number of complex

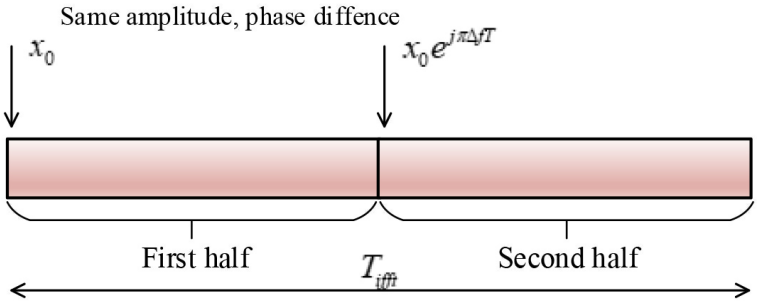

Figure 4-3: Schmidl's first symbol for timing

samples in one-half of the first training symbol is $N/2$ (excluding cyclic prefix), and summing up the pair of samples that are $N/2$ samples delayed, the sum of products is

$$P(d) = \sum_{m=0}^{N/2-1} (r^*_{d+m} r_{d+m+L}) \tag{4.10}$$

where d is a time index corresponding to the first sample in a sliding window of N samples. Then a timing metric can be difined as

$$M(d) = \frac{\left|P(d)^2\right|}{R^2(d)} \tag{4.11}$$

Performance and discussions of this timing algorithm will given by my colleague

Rui Shang, and the main focus here is frequency estimation which involves a second symbol. It contains PN sequence on even frequencies that are differentially modulated from the first symbol to help determine frequency offset. The two identical parts of the first symbol make it easy to detect differential phase the corresponding samples experience in the channel. It can be estimated by

$$\hat{\phi} = \angle(P(d)) \tag{4.12}$$

near the timing point. In [6], it is further developed that, if $\hat{\phi}$ is less than π, the offset estimate is:

$$\widehat{\Delta f} = \hat{\phi}/(\pi T) \tag{4.13}$$

otherwise, the even PN frequencies on the second training symbol will be employed for finding the actual frequency offset which will be

$$\widehat{\Delta f} = \frac{\phi}{\pi T} + \frac{2\hat{g}}{T} \tag{4.14}$$

where $\hat{g}$ is an integer number that indicates multiples the tone spacing obtained from the second symbol, [6]. It can be calculated by maximizing

$$B(g) = \frac{\left| \sum_{k \in X} x^*_{1,k+2g} v^*_k x_{2,k+2g} \right|}{2\left(\sum_{k \in X} |x_{2,k}|^2 \right)^2} \tag{4.15}$$

where X is the set of indices for the even frequency components. The advantage of this metric is surely its expanding the range for frequency offset detection, necessary for our project settings. But still, the updating speed may not be fast enough if we have long OFDM protocol frames. Also, the frequency estimates obtained at the start of frame needs to be refined for payloads, which will be discussed in the next section.

4.2 Improvements for both algorithms

Both of the two algorithms discussed in section 4.2 have their pros and cons. To briefly conclude, Sandell's algorithm can update estimate symbol-by-symbol, and the estimates may track along payloads better when the mobile station experience large accelerations, but it can't detect frequency offsets larger than half of tone spacing. Schmidl's metric requires less computation and can detect a large Doppler offset; yet it might not give very precise estimates in certain project settings.

In order to make this two algorithms more applicable for our project, we introduce some improvements for both that increase our system performance. Specifically, we expand the frequency detection range for the symbol-by-symbol Sandell algorithm, and added a differential frequency detector for Schmidl's estimator to to refine frequency estimates in low SNR cases.

4.2.1 Pilot-aided metric for expanding frequency detection range

In this subsection, we introduce a pilot-aided metric that expands Doppler detection range for Sandell's algorithm.

In Sandell's setting, it is illustrated in (4.13) that the correlation between $r(k)$ and $r(k+N)$ is $\sigma_s^2 e^{j2\pi\epsilon}$, and an estimatior for ϵ is given in (4.19). In Sandell's work, ϵ is indicated to have a range $-0.5 \leq \epsilon \leq 0.5$ to have a correct estimate of Doppler. ϵ beyond this range will appear to be a repetition, with an integer n being multiples of 2π. We call the portion of ϵ within this range as $\epsilon_{partial}$, so

$$e^{j2\pi\epsilon} = e^{j2\pi(\epsilon_{partial}+n)} \tag{4.16}$$

This means a large Doppler will appear to be a portion of the tone spacing in the estimator, which is why Sandell's estimator can only work for $\pm(1/2)F_{tone}$. However, complete Doppler offset can still be recovered from signal. Note that range of $\epsilon_{partial}$ may vary in different algorithms, which will be discussed later in this chapter. After partial despinning using $\epsilon_{partial}$, we are left with $e^{j2\pi n}$, where n is an integer number.

Again use notation in Sandell's metric, assuming we now have an offset of ϵ'

$$\epsilon' = \Delta f T = n, \quad n \in Z \tag{4.17}$$

where Z is the set of integer numbers. Therefore, Doppler offset in frequency is

$$\Delta f = \frac{n}{T} = n \cdot F_{tone} \tag{4.18}$$

(4.30) indicates after partial compensation, the remaining offset is just a multiple of tone spacings. One can get the correct shift by detecting shifts of pilots whose frequencies are known. In our project, pilot energy is twice as data energy, and can be detected at frequency domain by pilot indexes. Assuming at transmitter, a pilot index set has a total number of P pilots $\mathbf{P}_{idx} = [p_0, p_1, ..., p_{P-1}]$ to be inserted into OFDM symbol. These are subcarrier indexes. With Doppler offset $e^{j2\pi\epsilon}$ attached during transmission in time domain, according to the property of DFT, the DFT modulated signal will experience a shift in spectrum, the pilot set becomes

$$\mathbf{P}_{idx} + \epsilon = \big[p_0 + \epsilon, p_1 + \epsilon, ..., p_{P-1} + \epsilon\big] \tag{4.19}$$

After partial compensation, which means $\epsilon_{partial}$ has been compensated, the pilot set is left with a shift of n:

$$\mathbf{P}_{idx} + n = \big[p_0 + n, p_1 + n, ..., p_{P-1} + n\big] \tag{4.20}$$

So by shifting the spectrum of the Doppler partially corrected signal, one can find a maximum of the function below

$$\hat{n} = arg\max_n E(n) = arg\max_n \sum_{i=0}^{P-1} \big|p_i + n\big|^2 \tag{4.21}$$

The size of n can be chosen depending on project settings. In our case, we have $n \in \{0, \pm 1, \pm 2\}$, since one won't expect a Doppler shift of larger than two tone

spacings. Then we shift back the received spectrum with estimated $\hat{n}$, now frequency compensation has been completed, when $\Delta f > (1/2)F_{tone}$ for Sandell's procedure.

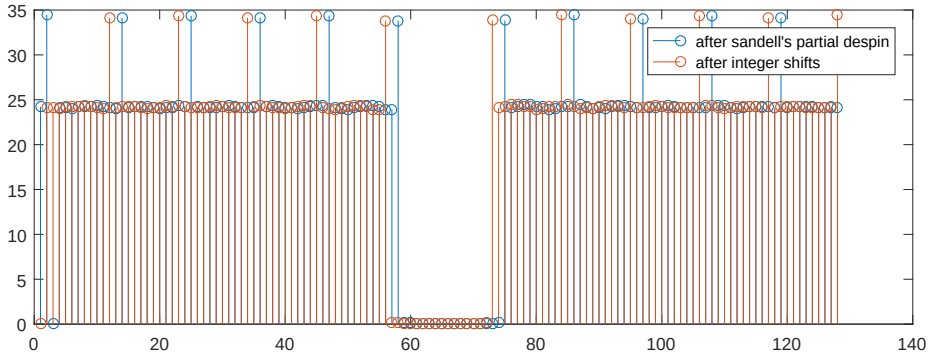

Figure 4-4: comparison between DFT demodulated signal before and after integer shifts

Figure 4-4 shows the spectrum signal with 15 kHz Doppler after DFT demodulations. Tone spacing is 7812.5 Hz. Both are partially compensated with Sandell's metric, since $\epsilon = \Delta f / f_{tone} = 15000\ kHz / 7812.5\ kHz = 1.92 = (2 - 0.08)$, so the spectrum needs to be left shifted after partial correction, as we can see from the blue spectrum to the red one.

4.2.2 Differential frequency detector for updating Doppler estimates

Both frame timing and frequency offset estimates in Schmidl's metric gets updated for each protocol frame, so this pair of estimate will be used for payload processing. In low SNR cases, the estimate is noisy and needs refinement for despinning payload symbols, which is one of motivations of differential phase detector. Another benefit is that it can track the changing Doppler offset in case when mobile stations have large accelerations, which is illustrated in Figure 3-8. This brings estimation errors for long protocol frames.

The differential frequency detector employs pilot signals. We model the kth pilot

at symbol m as

$$D(k,m) = H(k)\sqrt{2}e^{j\pi/4}e^{j\Omega\cdot(N+L)m} + N(k,m) \tag{4.22}$$

where Ω is the frequency error between the true Doppler and the S-C estimate that is applied to despin the received signal. $H(k)$ is the complex gain. $\sqrt{2}e^{j\pi/4}$ indicates the amplitude and phase angle pilots. $k = 0, 1, 2, ..., P-1$, and P is the number of pilots. To simplify, letting $\mathbf{D}$ be a vector of subcarriers corresponding to symbol index m,

$$\mathbf{D}(m) = \mathbf{H}(m)\sqrt{2}e^{j\pi/4}e^{j\Omega\cdot(N+L)m} + \mathbf{N}(m) \tag{4.23}$$

Assume every element in the vector has a common frequency rotation. Then we form

$$\mathbf{Z}(m) = \mathbf{D}(m)\cdot\mathbf{D}^*(m-1) = 2|\mathbf{H}|.^2 e^{j\Omega\cdot(N+L)} + \mathbf{N} \tag{4.24}$$

Summing the elements of $\mathbf{D}$(m) and taking its angle, and dividing by $(N+L)$ gives

$$\widehat{\Omega}_{diff}(m) = \frac{\angle\Big(\sum_P \big(\mathbf{Z}(m)\big)\Big)}{N+L} \tag{4.25}$$

where $\hat{\Omega}_{diff}$ is the estimated residual frequency error between S-C estimate and the true offset. Then we average out this noisy phase difference by

$$\overline{\widehat{\Omega}}_{diff}(m) = (1-\rho)\widehat{\Omega}_{diff}(m) + \rho\overline{\widehat{\Omega}}_{diff}(m-1) \tag{4.26}$$

with $\rho = 0.9$. Adding this averaged phase difference to Schmidl's estimate from start of frame gives a refined estimate of the frequency offsets.

4.3 Frequency unambiguous interval in OFDM systems

From algorithms discussed above, we observe that the frequency offset estimates come from a correlation of the received signal with it's delayed version. The difference in phase of two identical samples contains the frequency offsets. Related to this is an unambiguous interval of the frequency estimates, due to the periodicity of phase angles, which will appear in OFDM systems. Different delay of signal will have different unambiguous interval (Sandell's metric has a delay of N, while Schmidl's has a delay of $N/2$). This may affect algorithm designs for different projects.

Specifically, in Schmidl's method, the phase difference between two identical halves is

$$e^{j\phi} = e^{j\pi\Delta fT} = e^{j2\pi\frac{1}{2}\Delta fT} \tag{4.27}$$

For comparison, we use same notation in Sandell's metric discussed in section 4.2.1, $\epsilon = \Delta fT$, to refer the frequency offset relative to carrier frequency. Then we have a proper estimate when

$$-\frac{1}{2} \leq \frac{1}{2}\epsilon \leq +\frac{1}{2} \tag{4.28}$$

which yields $\Delta f \leq \pm 1/T = \pm F_{tone}$, where F_{tone} is the tone spacing. This means the range for unambiguity is twice than of Sandell's. The unambiguous interval often relates to tone spacing in OFDM systems, which is discussed in Appendix B, for the help of illustrations below.

- **Unambiguous Interval Analysis**

  Let the received signal be $r(k)$, and frequency offset be Δf, we have

$$r(k) = s(k-\theta)e^{j2\pi\Delta f\frac{k}{f_s}} \tag{4.29}$$

then we calculate a shifted version, shifted by arbitrary N:

$$\begin{aligned} r(k+N) &= s(k+N-\theta)e^{j2\pi\Delta f\frac{(k+N)}{f_s}} \\ &= s(k+N-\theta)e^{j2\pi\Delta f\frac{k}{f_s}}e^{j2\pi\Delta f\frac{N}{f_s}} \end{aligned} \tag{4.30}$$

If k is in a part where signal and its N samples delayed version are identical, we have $s(k-\theta) = s(k+N-\theta)$, so the difference between $r(k)$ and $r(k+N)$ is only a phase shift caused by Doppler frequency:

$$\frac{r(k+N)}{r(k)} = e^{j2\pi\Delta\frac{N}{f_s}}, k\ in\ CP\ interval \tag{4.31}$$

The phase shift from the righthand side of the equation above, has an unambiguous interval of 2π, i.e.

$$2\pi\Delta f\frac{N}{f_s} \tag{4.32}$$

has a period of 2π, which means $\Delta f\frac{N}{f_s}$ **has a unambiguous interval of 1**. Now we analyse the delay of N in each algorithm and determine the unambiguous interval of each with respect to tone spacing F_{tone}.

- (Sandell shift) In Sandell's algorithm [5] (4.7), the arbitrary shift N is equal to N_{ifft} (Sandell shift) and signal are same within CP, so we have:

$$\Delta f\frac{N}{f_s} = \Delta f\frac{N_{ifft}}{fs} = \Delta f\frac{1}{F_{tone}} = \epsilon \tag{4.33}$$

Therefore we have an unambiguous interval

$$|\epsilon| \leq \frac{1}{2};\ |\Delta f| \leq \frac{F_{tone}}{2} \tag{4.34}$$

- (Schmidl-Cox shift) In Schmidl-Cox's procedure [6], the first SC symbol has a repetition of 64, which is obtained from a 128-point FFT. So N_{ifft} is still 128, and the arbitrary shift N above here is $64 = N_{ifft}/2$ and is used for correlating

for frame sync. So the phase factor above is

$$\Delta f \frac{N}{f_s} = \Delta f \frac{N_{ifft}/2}{f_s} = \frac{\Delta f}{2F_{tone}} = \frac{\epsilon}{2} \tag{4.35}$$

Therefore, Unambiguous interval here is:

$$|\epsilon| \leq 1;\ |\Delta f| \leq F_{tone} \tag{4.36}$$

- (Minn shift) In Minn's method [16], a sequesce $[A\ A\ -A\ -A]$ is constructed for frame sync, and A is of length $N_{ifft}/4$. And correlation is computed by shifting length of $N_{ifft}/4$, therefore:

$$\Delta f \frac{N}{f_s} = \Delta f \frac{N_{ifft}/4}{f_s} = \frac{\Delta f}{4F_{tone}} = \frac{\epsilon}{4} \tag{4.37}$$

So we have an unambiguous interval:

$$|\epsilon| \leq 2;\ |\Delta f| \leq 2F_{tone} \tag{4.38}$$

As is indicated in section 4.3, when the partial frequency $\epsilon_{partial}$ has been estimated and compensated, the algorithm needs to detect the integer number of shifts the spectrum is left with. This can be done easily by searching for pilots, which is discussed in section 4.2.1. However, depending on project scenarios (vehicle speeds), if Doppler offset small, or within one tone spacing, there is no need for pilot aided resolution.

Chapter 5

Simulation Results and Analysis

In this chapter, simulation results will be presented, using root-mean-square error (RMSE) of frequency offset estimates for different algorithms and symbol error rate curves comparing with theory. At the begining, section 5.1 will illustrate the constellation plots with ambiguity interval resolution in Sandell's algorithm, and show estimator variance of the shifting estimate n in (4.20). Then in section 5.2, comparison of RMSE of estimates from Sandell's methods and Schmidl's will be presented and analysed.

5.1 Ambiguity resolving performance for Sandell algorithm

In this section, we show the simulation of pilot-aided shifting procedure for expanding the Doppler detection range, especially the shift index output after partial despinning in Sandell's method. The probability of making a shift error is presented as a function of E_b/N_0 in dB to show the performance and stability of this procedure.

5.1.1 Simulation and analysis of pilot shifting procedure.

It is shown in figure 4-4 that pilots may be shifted by an integer number of tone spacings after partial despinning. Then the power of pilots is used to detect the

correct shift. This indicates pilot amplitude to be important in this metric. Large pilot amplitude can certainly boost performance of this metric, even 0 error at low SNR. In our case, pilot symbols have a scale of $\sqrt{2}$ relative to QPSK symbols.

- 5000 Hz offset with respect to $F_{tone} = 7812.5\ Hz$. This is larger than one unambiguous interval of Sandell's metric, and it will produce a shifting index 1, as indicated in the Figure 5-1.

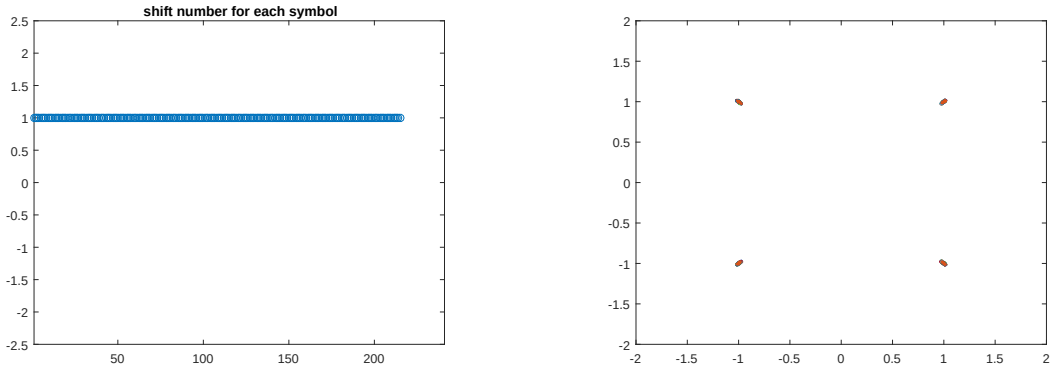

(a) Shifting number for each OFDM symbol

(b) Constellation after compensation

Figure 5-1: Unambiguous interval resolution for 5 kHz offset, one path, $E_b/N_0 = 60$ dB

- 15000 Hz frequency offset, since 15000 $Hz - 2 \times 7812.5\ Hz = -625 \in [-3906.3, +3906.3]$ Hz, it should appear in the second ambiguouos interval, see in Figure 5-2 (a).

- 11720 Hz frequency offset. This is a frequency at the boundary of ambiguous interval 1 and 2, and calculation gives

$$11720\ Hz - 2 \times 7812.5\ Hz = -3905\ Hz \in [-3906.3, +3906.3]\ Hz$$

With perfect estimation, the estimates should give the a shift of 2 tones, because from above calculation, $-3905\ Hz$ would be Sandell's estimation output, which is in the unambiguous zone of $\left[(-1/2)F_{tone}, (1/2)F_{tone}\right]$. But the estimates are in fact noisy. One can imagine these noisy estimates would jump back and force between the boundary. For example, if Sandell's estimator produce a frequency

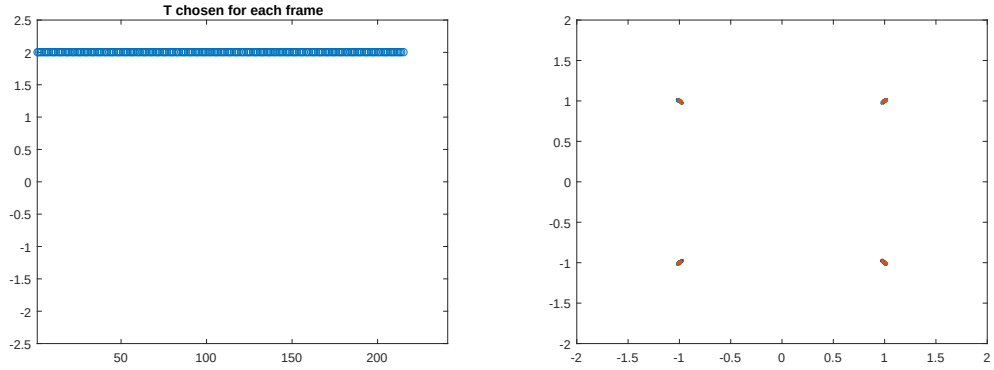

(a) Shifting number for each OFDM symbol (b) Constellation after compensation

Figure 5-2: Unambiguous interval resolution for 15 kHz offset, one path, $E_b/N_0 = 60$ dB

offset of 3905.5 Hz, which is 2 Hz off from the first calculation, is will sit on the upper boundary of the first ambiguous interval, giving a shift estimate of 1. The noisy frequency estimates from Sandell's procedure is given in Figure 5-3 (a), and correponding shifts Figure 5-3(b).

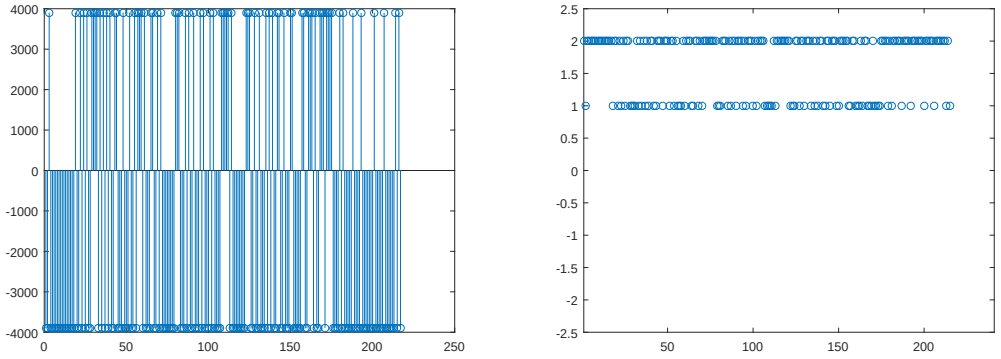

(a) Estimated frequency for each symbol, (b) Shifting number for each OFDM symbol within half of $\pm F_{tone}$

Figure 5-3: Unambiguous interval resolution for 11.72 kHz offset, one path, $E_b/N_0 = 60$ dB

Notice estimates of about -4000 Hz are more often, and gives a shift of 2, but estimates of about 4000 Hz don't mean there's 8000 Hz estimation error, they are in different ambiguous intervals, and the resolved estimates should just observe a few Hertz off. The constellation is given in Figure 5-4.

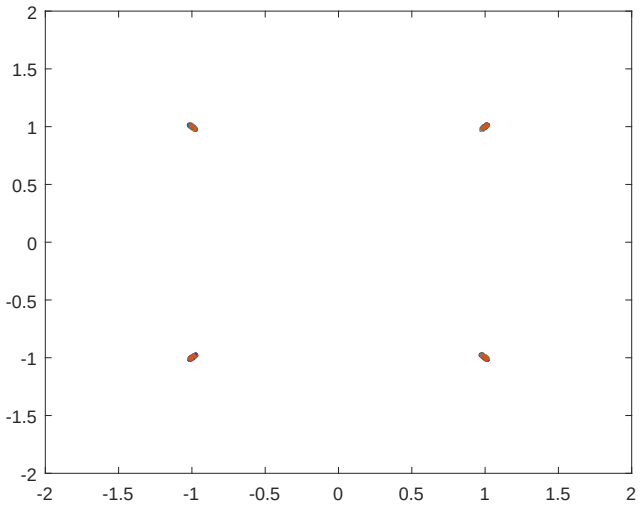

Figure 5-4: Final constellation for 11.72 kHz offset, one path, $E_b/N_0 = 60\ dB$

Cases above are all with $E_b/N_0 = 60\ dB$, one-ray. When the channel is a two-ray model, the signal will experience two Doppler shifts.

- Two-ray, 0.95 and 0.3 for each path, delay spread $2\mu s$. Doppler 6000 Hz (corresponding to speed of 1 Mach), and 4000 Hz. 60 dB constellations and shifts are given in Figure 5-5 (b). This model gives a 'noisy' constellation plot, but the scatterings are actually due to Doppler spread, not noise. The normalized frequency spread is $\epsilon = 0.25$. One may say that it doesn't check with the analysis of frequency error of 0.25 normalized offset in Chapter 3. This is due to two reasons. First is that the channel gain of the second path is small relative to the first one, so even if the second path is frequency synchronized badly, the scale's been reduced in the constellations. The second reason is that the frequency estimator will synchronize at some frequency between this two Doppler shifts, which reduces the normalized Doppler spread relative to it.

- Two-ray, $h(t) = 0.95\delta(t - 33\mu s) + 0.3\delta(t - 45\mu s)$, delay spread $12\mu s$, Doppler frequency 13600 Hz and 6800 Hz each. This approximately gives a model of a triangle with an angle of second path 60 degrees from the first path, with distance of aircraft to base station being 10 km and two Doppler shifts to be

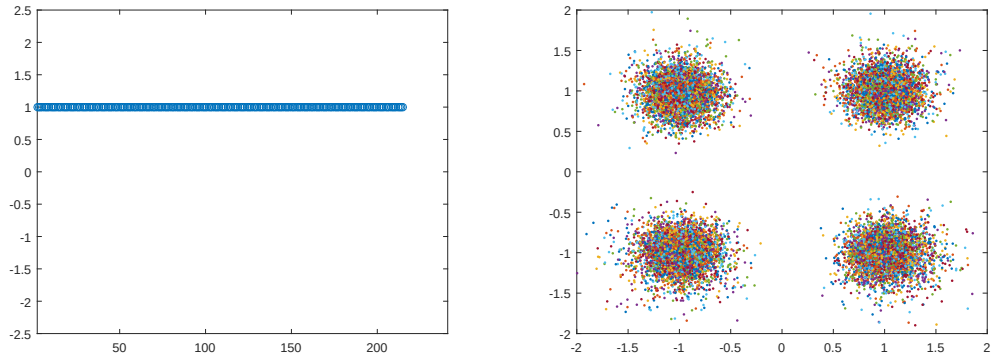

(a) Shifting number for each OFDM symbol (b) Constellation after compensation

Figure 5-5: Unambiguous interval resolution for two-ray multipath time-variant channel, 0.95 and 0.3 gains, delay spread 2 μs with offsets 6000 Hz and 4000 Hz, $E_b/N_0 = 60$ dB

13600 Hz, which is calculated from $Mach$ 2 as 680 $m/s \times \frac{3\times10^8}{6\times10^9}$ and 6800 Hz. This is a difficult case because the normalized Doppler spread is now 6800 Hz, which is $\epsilon = 0.87$.

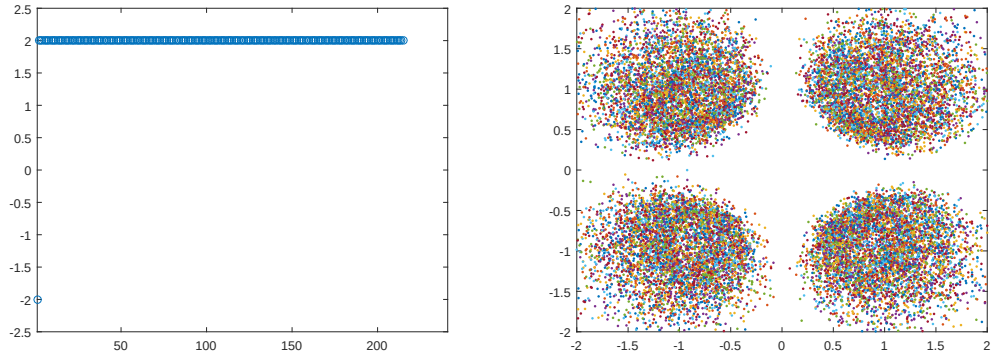

(a) Shifting number for each OFDM symbol (b) Constellation after compensation

Figure 5-6: Unambiguous interval resolution for two-ray multipath time-variant channel, 0.95 and 0.3 gains, delay spread $12\mu s$ with offsets 13600 Hz and 6800 Hz, $E_b/N_0 = 60$ dB

Consellations and corresponding shift are given in Figure 5-6. Note that even with normalized frequency $\epsilon = 0.87$, if the channel gain of the second path is small relative to the first one, Doppler spread can still be tolerable at high SNR. However, with presence of stronger noise, the error rate certainly increases

because of Doppler spread. This remains to be a tough case to handle and can be a research topic in the future.

5.1.2 Probability of making a shifting error (pilot amplitude is $\sqrt{2}$ for QPSK).

To indicate the performance of pilot-aided shifting procedure, we simulated one case of $E_b/N_0 = 1\ dB$, with a total number of 100 symbols, and plot the shift vs symbols in Figure 5-7 It is shown that there are 6 errors. These errors will introduce

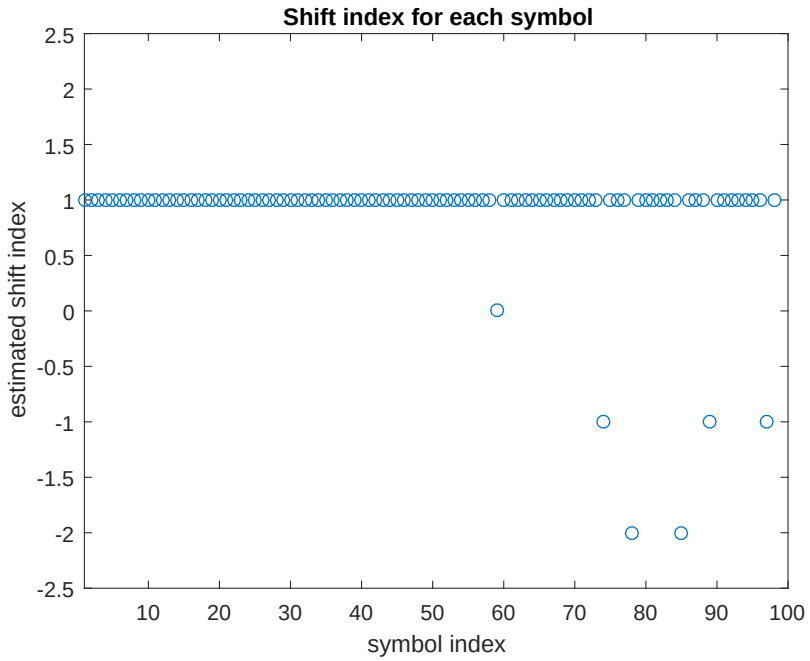

Figure 5-7: Estimated shift for each symbol, pilot amplitude is $\sqrt{2}$

large frequency error to the corresponding symbol. Performance of P_{error} will be given next.

To better illustrate the performance, we simulated a plot for probability of error shifts vs E_b/N_0,. In this simulation, transmitter generates 500 OFDM symbols and pass it through the channel with a frequency offset of $\Delta f = 5000$ Hz. We want the performance of pilot shifting metric, so we hardwire the receiver with a partial offset, or $\epsilon_{partial}$ of 5000 $Hz - 7812.5\ Hz = -2812.5\ Hz$. This means letting the partial

despinning by Sandell's procedure to be perfect, then the algorithm is left with a shift to estimate. The result is given in Figure 5-8. We notice that at 1 dB, the probability of making errors is less than 0.1, consistent with above. This suggests adequate performance will occur when $E_b/N_0 > 4\ dB$. Note that the estimate of shift is calculated from the summation of pilots. So with larger pilot amplitude, it will have more accurate estimation of shifts.

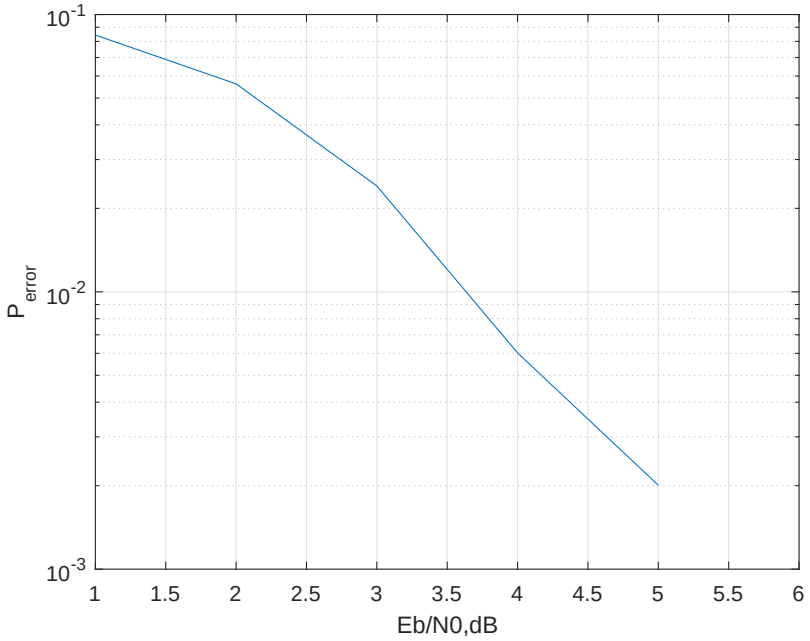

Figure 5-8: Probability of pilot-aided shifting error vs E_b/N_0, pilot amplitude is $\sqrt{2}$, QPSK

5.2 Comparison of frequency estimates between different estimators

This section compares performance of frequency offset in different algorithms, with constellation illustations and root-mean-square error (RMSE) vs $E_b/N_0,\ dB$.

5.2.1 RMSE plot comparisons

The system parameters used in these plots are given in Table 5.1. This is our previous system parameters, which are different from our current system in Appendix A.

Table 5.1: System settings

Number of OFDM symbols:	200
Total bandwidth	320 MHz
Lower sampling rate	10^6 MHz
FFT size	128
Subcarrier tone spacing	7812.5 KHz
Data subcarriers	100
Pilot subcarriers	11
Cyclic prefix length	14.6% (22 samples)

Figure 5-9 shows a comparison plot of RMSE of frequency estimates from both algorithms, with 11720 Hz frequency offset. From the figure we observe the RMSE of Sandell method to be about 0.65 of that of Schmidl method, indicating a slightly better performance. Figure 5-10 is a comparison plot of Schmidl's method only and

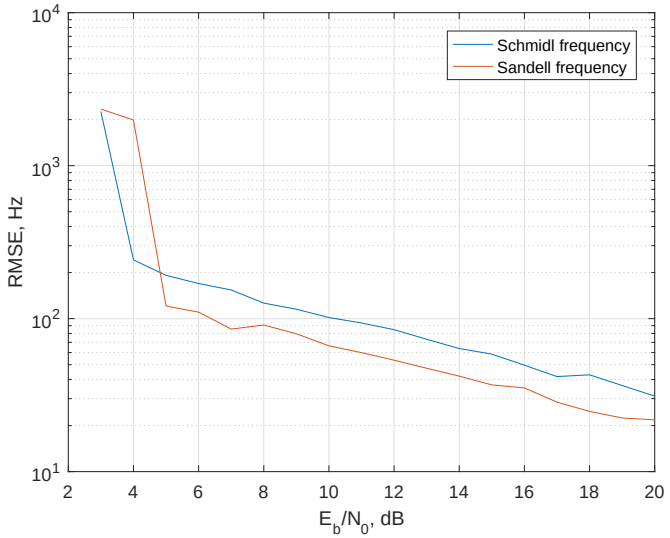

Figure 5-9: Comparison of RMSE of frequency estimates from two algorithms, $\Delta f =$ 11720 Hz

with differential averaging. Schmidl's procedure has one estimate for the whole pay-

load, a differential frequency detector serves as a good way to average out the noise. As one may see in Figure 5-10, it helps smooth Schmidl's noisy estimates and reduce the RMSE by a factor of about 8.5. Also, when channel geometry changes rapidly, it compensates for frequency offset error across protocol frames.

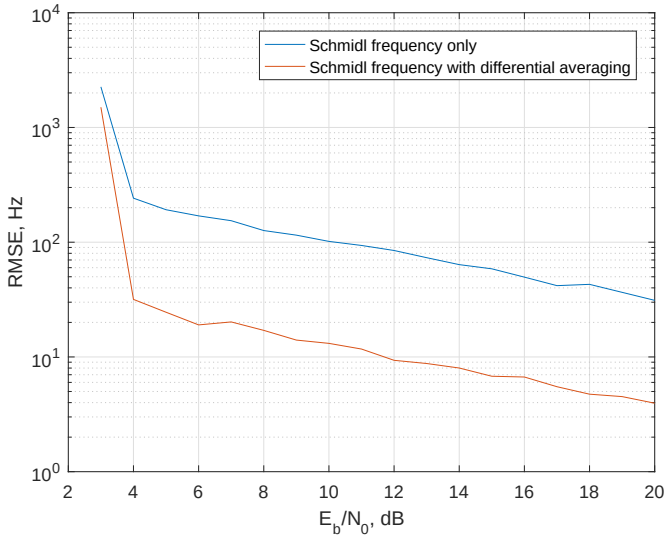

Figure 5-10: Comparison of RMSE of frequency estimate from Schmidl only and with differential averaging

5.2.2 Complexity

Computation requirements are important in evaluating an algorithm. We briefly analyse the computations required for these two algorithms. Assume we are sending an OFDM frame with M symbols, with two Schmidl's start of frame symbols at the beginning. The FFT size is N, cyclic prefix is L, so a total frame has $M(N+L)$ discrete samples. This includes P subcarriers. Assuming algorithm starts from the detection of signal power received that passes a threshold at the receiver, and ends at estimation of the timing index for a protocol frame.

With the assumptions above, freqeuency estimation in Sandell's method in (4.6) and (4.7) employs $3M(N+L)$ complex multiplications for correlation, which is $6M(N+L)$ real multiplications, $2M(N+L)L$ complex additions or $4M(N+L)$ complex addition for summation, Searching shifts for P pilots consumes MP complex

additions, or $2MP$ real additions and $4MP$ real multiplications, if we want n shifts including the $\pm F_{tone}$ zone, that's n times of one shift. So the total is $6M(N+L)+4nMP$ real multiplications and $4M(N+L)+2nMP$ real additions.

Frequency estimation in Schmidl's metric with two start-of frame symbols with length N has $N/2$ complex multiplications and $N/2$ complex additions. Searching for correct index g for n times in even frequency set $X = N/2$ requires another $nN/2 + N/2$ complex multiplications and additions, which in total gives $4N + 2nN$ real multiplications and $(n+1)N$ real additions. In addition to this, the differential phase detector employing pilots has MP complex multiplications for computing $\mathbf{Z}$, MP complex additions and M complex multiplications for $\hat{\Omega}$ and dividing. This in total gives $4N + 2nN + 4MP + 4M$ real multiplications and $(n+1)N + 2MP$ real additions. Note the shiftings for expanding the range in Schmidl's procedure computes power of $N/2$ subcarriers, for the second symbol, whereas Sandell's is computing P pilots for M payload symbols.

So Schmidl's algorithm with differential corrections is more feasible for project implementation in terms of computation requirements, and its performance is quite adequate, especially with differential pilot corrections.

5.2.3 Symbol error rate

Symbol error rate curves from different methods comparing with theory are given in Figure 5-11. The offset from the theory curve could be a small SNR calibration error, but the performance is quite simular for all methods. In our system, we've been working on Sandell's procedure for a long time, and achieved good results. After implementation Schmidl's procedure with differential averaging, we adopted this method. It requires much less computation, and we have verified through the models in Chapter 3 that the channel isn't changing that fast, so we do not need symbol-to-symbol updates in Sandell's procedure.

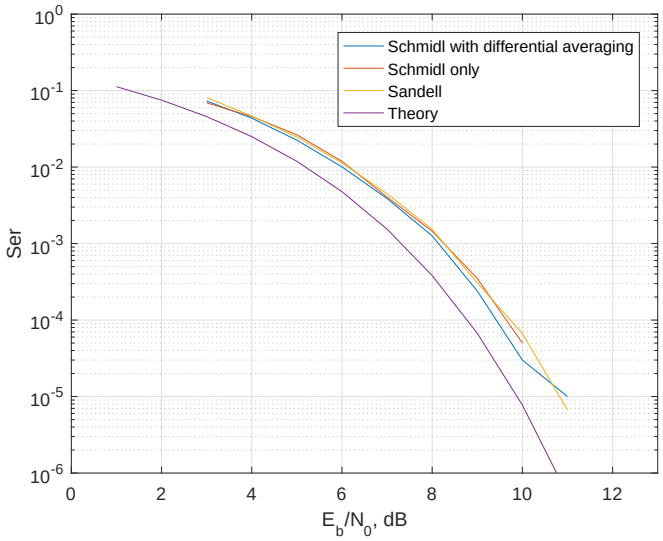

Figure 5-11: Symbol error rate comparison plot vs SNR

Chapter 6

Conclusions

In this thesis, we formulated and analysed the effect of frequency offset in OFDM communication systems. Frequency offset will introduce ICI to the demodulated signal and will produce noise-like scattering on constellations. Also, it will rotate the constellations, and the rotations appears to be accumulating across consecutive OFDM symbols. This can be taken care of by channel equalizations. We simulated some typical and extreme case models to determine whether estimates produced by previous algorithms serve our project. Analysis shows that the aircraft turning and two-ray time-variant channel introduce Doppler shift and spread that are not significant.

Then we introduced two previous frequency estimation algorithms and compared them. Growing from this, we gave a generalized discussion of frequency unambiguous interval for frequency offsets for different algorithms. The ambiguous interval will be needed for cases having frequency offset larger than a range, which is determined by the shifts of samples in different algorithms. After that, we compared algorithms in terms of estimator RMSE, and complexity, and introduce improvements for both to better serve our project. For Sandell's metric, we expand the range of frequency offset detection, and for Schmidl's, we implemented a differential frequency detector to refine the noisy estimates of the frequency. At last, Schmidl's algorithm with differential phase corrections is preferred for our project.

6.1 Future work

As is indicated in Chapter 5, large Doppler spread with high SNR will distort the constellations, and it is still a tough case to handle for algorithms, since the estimator can only synchronized at a "mean" frequency, which gives bad offset correction for other paths with different frequency offsets. Future work on frequency offsets includes design of algorithms for large Doppler spreads.

From Sandell's [5] algorithm to Schmidl's [6], and to Minn's [16], we observe a common thread of exploiting correlations between the signal and its delayed version. The delay is designed for better frame sync estimates in those methods, but it also serves for estimating the frequency, relating to the unambiguous interval as discussed in Chapter 4 and 5. So in terms of frame-by-frame estimations, design of start-of-frame symbols to improve timing and frequency estimates is another research question.

Appendix A

Overview of project context for research (S.G. Wilson)

This research was sponsored by Laulima Systems, under contract to the National Spectrum Consortium, with the intent of providing enhanced spectral efficiency for Air Force telemetry test ranges, along with opportunities to utilize new, but already assigned C-band spectrum, on a non-interference basis. The adopted scheme is to use up to eight OFDM carriers placed on 2 MHz centers across the C-band region, using frequencies chosen to avoid interference with legacy users.

Each OFDM carrier has a clock rate of 1.6 Msps at the output of CP insertion, and with pulse shaping the RF spectrum fits within the 2 MHz interval. The FFT size for each OFDM carrier is 128, giving a tone spacing of 12.5 kHz. Eight guard subcarriers are used on each edge for avoiding channel overlap. With the zero-frequency channel also dropped for reasons of DC offset, and $P = 11$ pilots chosen, the payload consists of 100 active data subcarriers in each OFDM symbol. With QPSK modulation, 200 bits are sent in a symbol duration, including CP of length 22 samples, of 93.75 microseconds, producing a data rate, per carrier, of 2.13 Mbps. With eight OFDM carriers active, the air-to-ground data rate is 17.0 Mbps.

The transmission protocol organizes emissions into frames of duration 30 milliseconds. In each frame we assign 6 OFDM intervals of silence, for differential propagation guard time, 2 Schmidl-Cox start-of-frame symbols, 280 payload symbols, 16 symbols

where the aircraft sends probe signals to the base station to measure channel quality over multiple frames, and finally 14 symbols of silence for radio silence to determine channel activity by legacy users on all available channels. Frames repeat on 30 millisecond boundaries. The uncoded throughput per channel is thus (200)(282) bits 30 milliseconds, or 1.88 Mbps.

While most of the research and development reported in this thesis is generic to OFDM technology, some of the parameter choices and simulation values are driven by the project design. Moreover the work on handling large Doppler offset, and processing signals with very low SNR are motivated by project demands.

The figure below is summarizes important parameters of the multicarrier OFDM design. [17]

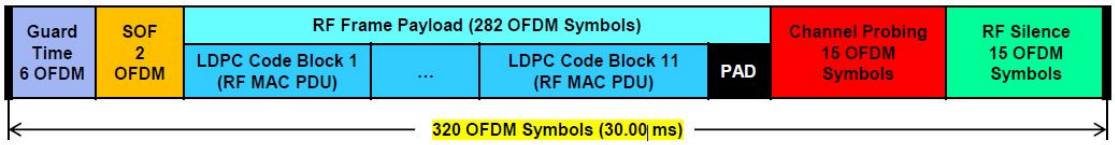

	Value	Units		Value	Units
Channel Spacing	2.00	MHz	Guard Time	6	OFDM Symbols
CP Insertion	1.60	MHz	SOF	2	OFDM Symbols
FFT	128	samples	Frame Payload	282	OFDM Symbols
Cyclic Prefix Extension	22	samples	Channel Probing	15	OFDM Symbols
Samples per OFDM Symbol	150	samples	RF Silence	15	OFDM Symbols
OFDM Symbol Length	93.75	microseconds	Frame Length	320	OFDM Symbols
OFDM K Symbols per second	10.67	KSPS	Frame Time	30.000	milliseconds
Bits Per Symbol (QPSK)	2	bits/symbol	Bits per Frame (raw)	64000	bits
Active Carriers	100		LDPC Code Block Size (unencoded)	4096	bits
Bit Rate per Channel (raw)	2.13	Mbps	LDPC Coding Rate	0.80	4/5 encoding
Max TA Transmit Channels	8		LDPC Code Block Size (encoded)	5120	bits
Max TA Transmit Bit Rate (raw)	17.07	Mbps	RF Frame Data Payload Size (encoded)	56400	bits
Max TA Transmit *RF MAC PDU Bit Rate*	12.01	Mbps	LDPC Code Blocks per Frame	11	LDPC code blocks
Max Available Bandwidth	320.0	MHz	RF Frame Data Size (encoded)	56320	bits
Number of Possible Channels	160.0	channels	RF Frame Pad Size	80	bits
Notes:			RF Frame Data Size (unencoded)	45056	bits
1 frame every 30 ms			***RF MAC PDU Bit Rate* (unencoded)**	1.50	Mbps
100 frames every three seconds			OFDM Symbols in three seconds	32000	OFDM Symbols
Frame always on 0.0, 3.0, 6.0, etc. boundary			Frames per three seconds	100.00	frames

Note: yellow highlighted fields are calculated values.

Figure A-1: Protocol frame

Appendix B

Tone spacing calculation

Tone spacing is the subcarrier spacing in OFDM systems, the calculation of tone spacing is critical, for determine frequency offsets in OFDM systems. Appendix B illustrates the calculation of tone spacing. Tone spacing is the reciprocal of IFFT time T_{ifft} which is N_{ifft} samples at sampling rate f_s.

$$F_{tone} = \frac{1}{T_{ifft}} = \frac{1}{N_{ifft} \cdot \frac{1}{f_s}} \tag{B.1}$$

so we have:

$$\frac{N_{ifft}}{f_s} = \frac{1}{F_{tone}} \tag{B.2}$$

In our previous system design, the lower sampling rate is $f_s = 1MHz$. At this sampling rate, $N_{ifft} = 128$ so

$$F_{tone} = \frac{1}{T_{ifft}} = \frac{1}{128 \times \frac{1}{1\times10^6}} = 7812.5\ kHz \tag{B.3}$$

In our current design, the lower sampling rate is 1.6 MHz. So the tone spacing F_{tone} is (note N_{ifft} is still 128):

$$F_{tone} = \frac{1}{T_{ifft}} = \frac{1}{128 \times \frac{1}{1.6\times10^6}} = 12.5\ kHz \tag{B.4}$$

Considering this with higher sampling rate 128 MHz: the lower sampling rate of

1.6 MHz is upsampled by 5 and then 16 to 128 MHz. So calculating F_{tone} (note N_{ifft} is still 128):

$$F_{tone} = \frac{1}{T_{ifft}} = \frac{1}{128 \times 5 \times 16 \times \frac{1}{128 \times 10^6}} = 12.5\ kHz \tag{B.5}$$

Bibliography

[1] S. B. Weinstein. "The history of orthogonal frequency-division multiplexing". *IEEE Communications Magazine*, 47:26–35, 2009.

[2] Y. Wu and W. Y. Zou. "Orthogonal frequency division multiplexing:a multi-carrier modulation scheme". *Proceedings of International Conference on Consumer Electronics*, page 8, 1995.

[3] S. Weinstein and P. Ebert. "Data transmission by frequency-division multiplexing using the discrete fourier transform." *IEEE Transactions on Communication Technology*, 19(5):628–634, October 1971.

[4] C. Fan and L. Cao, "Principles of Communications", *National Defense Industry Press*, 2012, pp.252

[5] M. Sandell, J. van de Beek, and P. O. Borjesson, "Timing and frequency synchronization in OFDM systems using the cyclic prefix," in Proceedings: *1995 International Symposium on Synchronization*, Saalbau, Essen, Germany, December 14-15, 1995, 1995, pp. 16-19.

[6] T. M. Schmidl and D. C. Cox, "Robust frequency and timing synchronization for OFDM," in *IEEE Transactions on Communications*, vol. 45, no. 12, pp. 1613-1621, Dec 1997.

[7] Y. R. Kwok; V. K. N. Lau, "The Mobile Radio Propagation Channel," in *Wireless Internet and Mobile Computing:Interoperability and Performance* , 1, Wiley-IEEE Press, 2007, pp.664-

[8] S. Haykin and M. Moher, "Modern Wireless Communication." Prentice-Hall, Inc., Upper Saddle River, NJ, USA, 2004.

[9] S. Zhou; Z. Wang, "OFDM Basics," in *OFDM for Underwater Acoustic Communications*, 1, Wiley Telecom, 2014, pp.

[10] M. A. Deshmukh and S. G. Wilson, "Channel estimation in OFDM: Interpolation versus ESPRIT," *2018 IEEE 8th Annual Computing and Communication Workshop and Conference (CCWC)*, Las Vegas, NV, 2018, pp. 673-678.

[11] S. G. Wilson, R. Shang and R. He, "Frame synchronization for OFDM using cyclic prefix and pilot carriers," *MILCOM 2017 - 2017 IEEE Military Communications Conference (MILCOM)*, Baltimore, MD, 2017, pp. 214-218.

[12] 3GPP TS 36.214: "Evolved Universal Terrestrial Radio Access (E-UTRA); Physical channels and modulation".

[13] M. M. A. Moustafa and S. H. A. El-Ramly, "Carrier frequency offset compensation using radial basis networks for OFDM systems," *2009 1st International Conference on Wireless Communication, Vehicular Technology, Information Theory and Aerospace and Electronic Systems Technology*, Aalborg, 2009, pp. 698-701.

[14] P. Malarvezhi and R. Kumar, "A modified preamble structure based carrier frequency offset (CFO) compensation in an OFDM system," *2013 International Conference on Communication and Signal Processing*, Melmaruvathur, 2013, pp. 504-508.

[15] W. Zhiqiang, B. Haixia and Z. Zichao, "A channel analysis method for ground-air wireless communication system," *2017 IEEE 17th International Conference on Communication Technology (ICCT)*, Chengdu, 2017, pp. 156-159.

[16] H. Minn, M. Zeng and V. K. Bhargava, "On timing offset estimation for OFDM systems," *in IEEE Communications Letters*, vol. 4, no. 7, pp. 242-244, July 2000.

[17] C. Reinwald, "ASAM System Overview", Laulima Systems, March 18, 2018